NASA CONTRACTOR REPORT

NASA CR-54194

NASA CR-54194

VAPOR-FILLED THERMIONIC CONVERTERS

Prepared by K. G. Hernqvist *(Project Engineer)*, J. R. Fendley, and J. D. Levine

Approved by P. Rappaport, *Project Supervisor*

MID-POINT REPORT

Prepared under Contract No. NAS 3-4173

RADIO CORPORATION OF AMERICA
RCA LABORATORIES
PRINCETON, NEW JERSEY

for

NATIONAL AERONAUTICS & SPACE ADMINISTRATION • CLEVELAND, OHIO • SEPTEMBER 1964
LEWIS RESEARCH CENTER

FOREWORD

This report includes theoretical and experimental results from study of cesium surface adsorption and cesium plasma phenomena. Section I was prepared by Dr. J. D. Levine, Section II by Dr. K. G. Hernqvist and Section III by Mr. J. R. Fendley, Jr.

We wish to acknowledge the encouragement and support of Mr. Harold Nastelin and Mr. Herman Schwartz of NASA Lewis Laboratories.

ABSTRACT

33100

Electrical conductivity due to cesium adsorption on insulators has been studied extensively. For "clean" ceramic systems (defined roughly as continuously gettered systems, or closed systems in initial stages of life) conductivity of adsorbed cesium in equilibrium with cesium vapor follows a simple Arrhenius law. For "unclean" systems (defined roughly as closed systems in later stages of life where gases can accumulate) conductivity is larger and obeys a similar law. Conductivity kinetic studies show that conductivity is proportional to the fourth power of arrival rate and of time after admitting a cesium beam. But the first half monolayer of adsorbed cesium becomes electrically inert due to cesium traps. Activation energies for cesium ionization and cesium diffusion have been calculated from analyzing temperature coefficients of conductivity and conductivity drifts after shutting off the cesium beam. The above data serve as a basis for extracting cesium interactions, conduction mechanism, and binding mechanism.

Plasma phenomena affecting the volt-ampere characteristic of the arc mode thermionic converter are discussed. Based on the ball-of-fire theory and including reverse current effects, an analysis is presented which yields a relation between arc drop and the pressure spacing product. It is shown that minimum arc drop in general does not coincide with minimum electron temperature.

Probe measurements of electron temperature are described. The measurements indicate electron temperature in the 3000 to 4000°K range.

Various measurements of arc drop and anode work function are reported. Arc drop is found to be nearly 0.5 volt for cathode temperature in the range 1300 to 1500°K and current density of 6 to 12 amp/cm^2. Anode work function with a high cesium coverage has been found to be equal to or greater than 1.93 volt.

Author

TABLE OF CONTENTS

LIST OF ILLUSTRATIONS

LIST OF ILLUSTRATIONS (Continued)

I. ADSORPTION OF CESIUM ON INSULATORS

A. MOTIVATION FOR STUDYING CESIUM ADSORPTION ON INSULATORS

The adsorption system of cesium on insulators is in many ways ideal for experimental research. Because there is little chemical reaction between cesium and insulators, the data are largely reproducible. Because a great variety of properties can be measured, such as electrical conductivity, surface ionization energy, thermoelectric effect, diffusion, and kinetics of adsorption, the system is versatile. Finally, because the insulator substrate is electrically inert, electrical effects caused by adsorbed cesium can easily be distinguished from the bulk and observed over many orders in magnitude.

The goal of this study is to monitor electrical properties of adsorbed cesium, and then to deduce the electron distribution within the cesium-substrate bond, and the electrical cesium-cesium interactions. Such deductions are not possible if more conventional techniques are used. For example, thermionic emission only gives work function, field ion microscopy only gives adsorbate position on a crystal lattice, low energy electron diffraction only gives ordering of adsorbate aggregates, etc.

In the past, many theoretical models of adsorption have been proposed concerning metal-insulator or metal-semiconductor systems. Weisz[1] considers an adsorbate such as cesium to be bound as an ion with an initial binding energy equal to work function minus vapor ionization potential (3.9 ev). This energy is supposed to decrease parabolically with coverage until about 0.005 monolayer when no more cesium can be adsorbed. The decrease is supposed to be caused by band-bending of the substrate, and each electron donated by the cesium is supposed to go into the conduction band of the insulator. Similar, though more general, concepts have been forwarded by others such as Sandomirski,[2] Kogan,[3] Krusemeyer,[4] Heiland,[5] and Boudart.[6] Some of these workers include complications of surface states, non-zero donor energies and degenerate electron gases, but all have in common adsorbate ionization and band-bending of the substrate. Other workers such as Mott,[7] Dowden,[8] and Vol'kenshtein[9] do not stress band-bending but instead focus attention on strong localized adsorption bonds. Benjamin[10] and Rhodin[11] consider a metal-insulator bond to be caused by weak non-localized Van der Waals forces. Frenkel[12] and Walton[13] propose grouping of two adsorbate atoms to form a diatomic species which is

more stable than two single atoms; it may also serve as a nucleus for further film growth under certain conditions. Neugebauer[14] considers adsorbate or adsorbate cluster interactions to occur by activated tunnelling, and Nifontoff[15] considers adsorbate or adsorbate cluster interactions to occur via a monatomic layer of non-removable surface contaminant. Lovell and Appleyard[16] consider diffusion, stresses and surface tensions in the cesium film formations. Conwell[17] considers weak interactions to form an impurity band. Blackford[18] and the present writer[19] have noted that cesium conductivity is proportional to cesium pressure squared, in dynamic equilibrium. This strongly indicates[19] a model of diatomic cesium adsorption in agreement with the ideas of Frenkel.[12]

Although many theoretical models mentioned above have been proposed, there is a lack of well-defined and reproducible experimental data for comparison. The main purpose of this report is to add to the available data of cesium adsorption on insulator systems.[16,18,19] Some theoretical interpretations will be forwarded, but a more complete theoretical analysis will appear in the Final Report.

The particular applicability of the cesium-insulator effort to cesium thermionic energy conversion is threefold. First, empirical conductivity data at high cesium temperatures and surface temperatures may aid in the choice and operating conditions of insulators in cesium converters. Second, the adsorption properties of cesium on insulators may prove useful in understanding the nature of present-day low work function anodes. For example, there is evidence that observed low work functions ~1.4 ev are characteristic of cesium plus metal substrate plus electronegative contaminant such as O_2. But is cesium adsorbed in the form of (a) a free cesium atom on an oxidized metal substrate, or (b) a cesium oxide molecule loosely bound to a pure metal substrate? The present study considers cesium adsorption on an oxidized metal, Al_2O_3, so (a) may be critically evaluated. Finally, the cesium-cesium lateral interactions which can be inferred from the present effort provide one of the missing links in understanding cesium-metal adsorption systems at coverages near one monolayer.

The report is arranged as follows: Section I-B is an extension of previous measurements of surface conductivity in dynamic equilibrium with cesium vapor. Next, we discuss a newly built cesium beam device which deposits cesium at a controllable rate on a low temperature sapphire substrate. Measurements of conductivity at various times after opening and closing the cesium

beam shutter at different sapphire temperatures yield conductivity kinetics, temperature coefficient, and surface diffusion in Section I-C, I-D, and I-E, respectively. In Section I-F preliminary thermoelectric measurements, Hall measurements, ohmic measurements, and pulse measurements give additional information. A summary of the pertinent results is given in Section I-G, together with a plan for future work.

B. SURFACE CONDUCTIVITY IN DYNAMIC EQUILIBRIUM WITH CESIUM VAPOR

A new series of investigations was carried out to see if conductivity data[19] previously obtained for cesium on moderately compatible Diamonite P-3142 high alumina ceramic are applicable to other substrates. The two substrates chosen were Frenchtown 4462 high alumina ceramic and sapphire (crystalline Al_2O_3) because they are supposed to be respectively incompatible and compatible with cesium throughout the temperature conditions of the tests.[20]

In these experiments a dynamic equilibrium is set up between adsorbed cesium on an insulator surface at temperature T and cesium vapor in contact with a liquid reservoir at a lower temperature T', as shown in Fig. 1. The adsorbed cesium causes an electrically conducting path to be formed which can

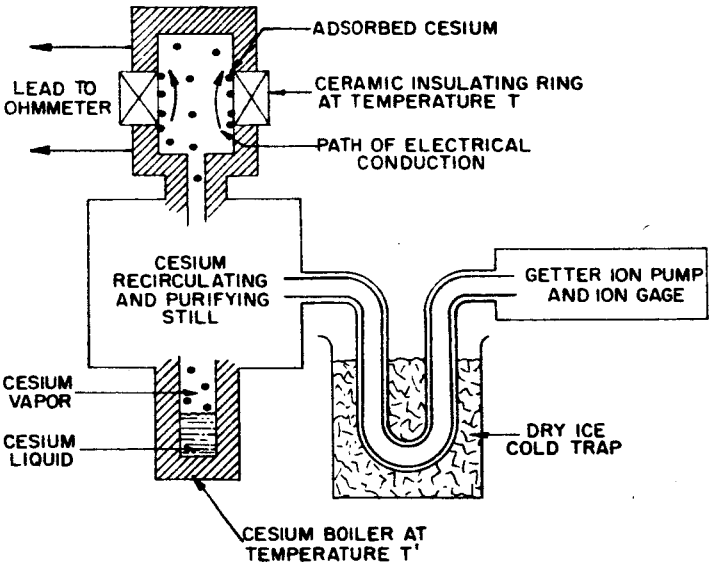

Fig. 1. Schematic experimental arrangement for measuring surface conductivity as a function of T and T'. Conductivity proceeds via the adsorbed cesium film. The purifying still, cold trap and getter ion pump remove contaminant gases.

be conveniently monitored by an ohmmeter. For Diamonite P-3142 the surface conductivity per square, $g_{\square}$, was found to obey the semiempirical equation

$$\log g_{\square} = A - B/T' + C/T \text{ mhos/square} \quad (1)$$

where

$$A = -5.4,\ B = 7520,\ C = 8340. \quad (2)$$

The object of the experiments to follow was to see if the Frenchtown and sapphire substrates obey Eq. (1) with A, B, and C values similar to Eq. (2). A review is also made of Blackford's[18] cesium on Pyrex glass data, to see how it compares with these equations.

Note that if a family of curves can be put into the form of Eq. (1), then there is unquestionably only one contribution to the conductivity, namely that due to the adsorbed cesium. An assumed sum of effects such as surface and volume conductivities cannot be represented by Eq. (1) over many orders in magnitude. These considerations which clarify the isolation of one effect were not recognized previously.[19]

1. Cesium Adsorption on Frenchtown Ceramic

a. Experimental Arrangement

Two Frenchtown #4462 ceramic discs with a 3/4-inch inner diameter and a 3/16-inch thickness were chosen as insulators as shown in Fig. 2. They were mounted one on top of the other and soldered to a Kovar tube. The solder was silver-copper eutectic. Three electrical leads allowed measurement of conductivity across either of the two ceramics. The Kovar tube was connected to a copper tube through an intermediate Frenchtown insulator. Finally, the copper tube was connected to a flange and operated in a cesium still and getter ion pump arrangement[19] shown in Fig. 1. Provision was also made for distilling cesium into the copper tube so that it could be pinched off (dashed lines in Fig. 2) and isolated from the cesium still and getter ion pump.

b. Contaminant Gases

Since contaminant gases would be continuously removed by the cesium still and getter pump arrangement, but would accumulate after the tube was pinched off, a preliminary study was made to determine the pressure of the contaminant gases. The study was carried out by varying the cesium reservoir temperature and noting the pressure at the getter ion pump shown in Fig. 1. A dry ice trap allowed no cesium to reach the pump. The contaminant gas noted at the pump was probably hydrogen as inferred from previous mass spectrometer tests.

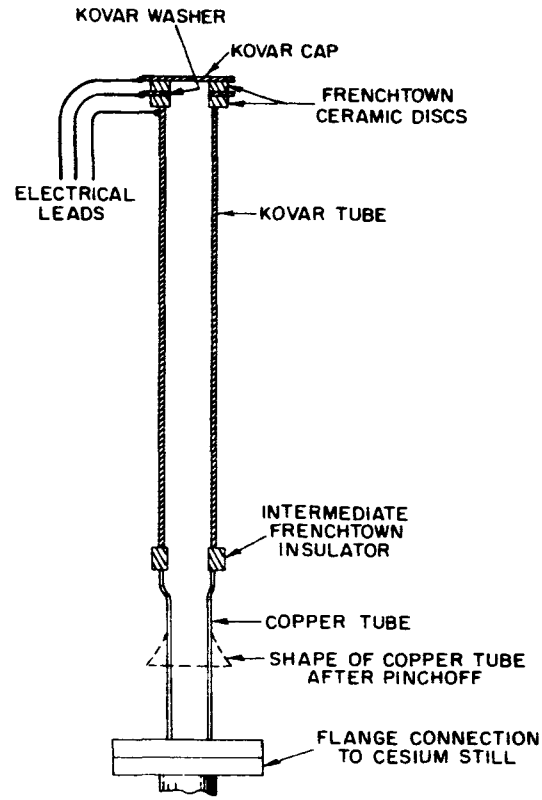

Fig. 2.
Tube used for measuring conductivity of cesium films adsorbed on Frenchtown ceramic. Dynamic equilibrium is established between adsorbed cesium and cesium vapor.

Plots of contaminant pressure versus cesium pressure (calculated from T') are shown in Fig. 3. The data can be represented by the following empirical equation

$$\log P_H = -6.3 + 0.5 \log P_{Cs} \qquad (3)$$

where the contaminant pressure P_H (probably hydrogen) and the cesium pressure P_{Cs} are expressed in Torr units. If the contaminant is presumed located in cesium liquid then it follows from Eq. (3) that the contaminant evaporation energy ϕ_H is related to the cesium evaporation energy ϕ_{Cs} by

$$\phi_H = 0.5\ \phi_{Cs} = 0.4 \text{ ev} \qquad (4)$$

which is similar to the vaporization heat (0.5 ev) of hydrogen from cesium hydride. Because of various gettering actions of the dry ice trap and because of pumping actions of the cesium still, these data are only an estimate. Yet there is definitely a one-to-one correspondence as shown by the straight line in Fig. 3 over five orders in magnitude. One concludes that before pinching the

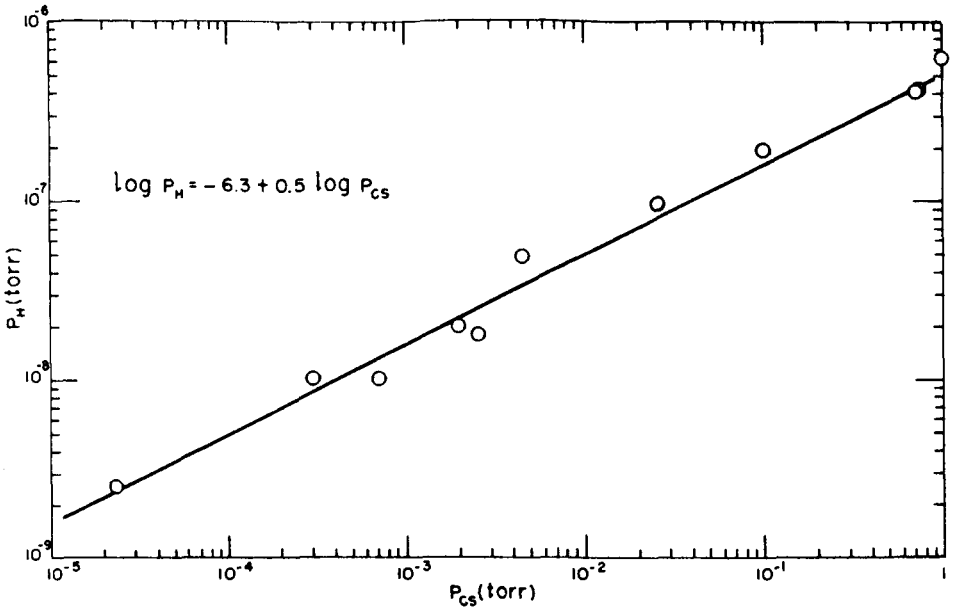

Fig. 3. Contamination pressure P_H noted at ion gauge versus cesium pressure P_{Cs} calculated from bath temperature. Data apply to a continuously gettered system, not to a closed-off system.

copper tube off, the ratio of contaminant pressure to cesium pressure was about (10^{-4} to 10^{-6}) over a cesium pressure range of 10^{-5} to 1 Torr. After pinchoff of the copper tube, the contaminant pressure probably became greater, but there was no means for its measurement.

c. Data Before Pinchoff

Before pinching off the copper tube, data shown in Fig. 4 was taken with the cesium still and getter ion pump ("Vacion") in continuous operation. The two Frenchtown ceramics had conductivities agreeing within about 10 percent. To show how the data was taken, consider run #9 for example. The other runs, #6, 7, 8, 10, 11 and 14, shown similar behavior. In run #9 the bath temperature was fixed at T' = 471°K. Data were taken by letting T decrease slowly from 700°K to 471°K as shown by the points ▲. Reversed data were taken with T increasing slowly from 471°K to 495°K as shown by the points ▼. There is no hysteresis.

For T higher than 520°K there is curvature in the data. It was discovered later that this curvature could be largely removed by applying a magnetic field, showing that the main cause for the curvature is probably thermionic conductivity from one metal electrode to the other, through the vapor space. (See

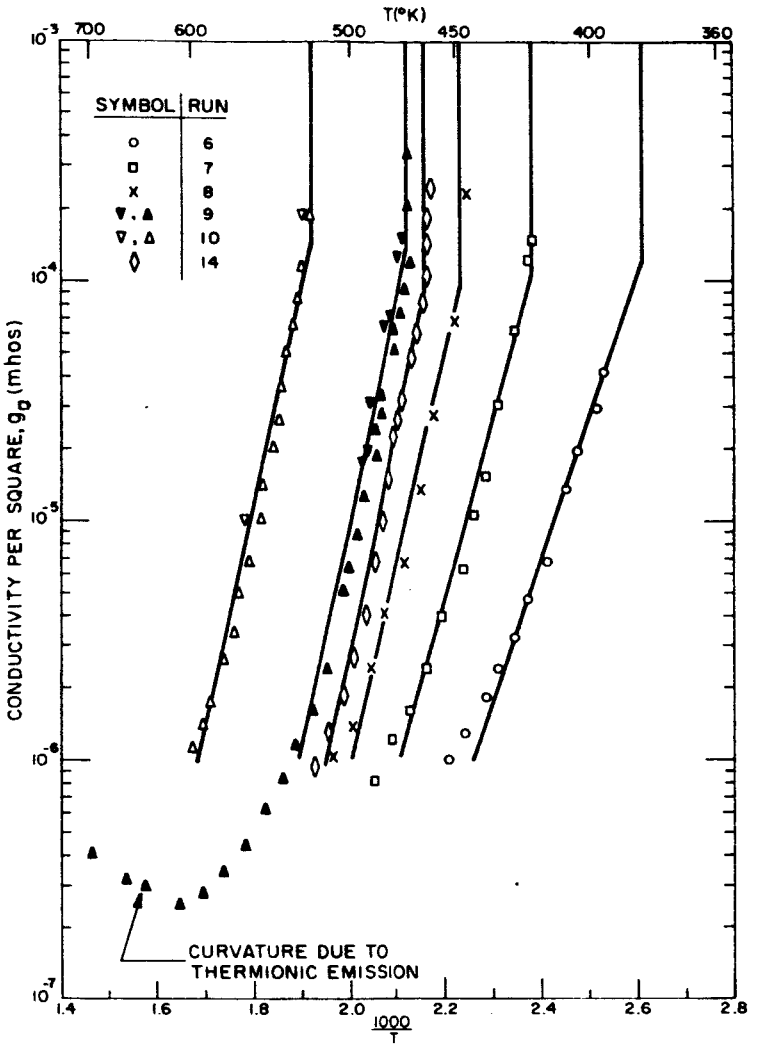

Fig. 4. Conductivity versus reciprocal surface temperature for cesium on Frenchtown ceramic with getter ion pump on. Each run corresponds to a different cesium bath temperature given by the vertical line. Rapid mass condensation occurs when surface and bath temperatures are identical.

pages 10 through 12.) Thus, it is felt that the surface conductivity data presented are ohmic and reliable only for $g_\square > 10^{-6}$ mho/square, where the conductivity follows an exponential increase for two decades. Finally, for T = T', bulk cesium condensation occurs and the conductivity rises at constant temperature to about 1 mho/square; the rise is shown by the vertical line in the figure. Apparently, there is little or no supersaturation required to cause bulk condensation as is the case for systems such as Cd and Hg on glass.[10] Rapid bulk condensation can be observed, however, only if the cesium pressure is high enough for rapid mass transfer.

A cross plot of these data is shown in Fig. 5. Values of constant conductivity (▼, ■, and ▲ for 10^{-4}, 10^{-5}, and 10^{-6} mho, respectively) are shown with 1000/T as ordinate and 1000/T' as abcissa. Also on the same plot are previously reported data for cesium on Diamonite ceramic (▽, □, △, and o for 10^{-4}, 10^{-5}, 10^{-6} and 10^{-7} mho, respectively) and also some data for cesium on sapphire to be discussed later. The straight line family is semiempirical with two adjustable parameters.[19]

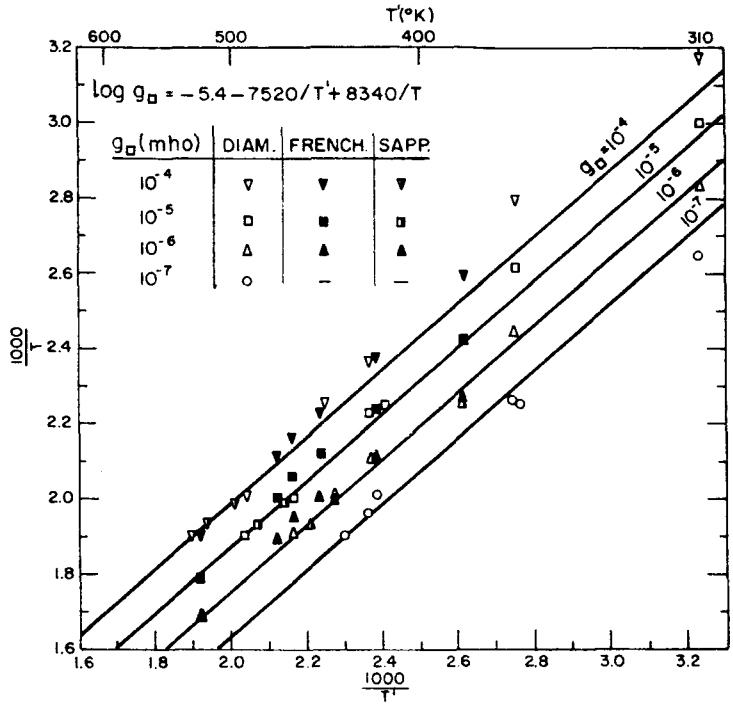

Fig. 5. Master plot of constant conductivity versus reciprocal bath and surface temperatures, taken under "clean conditions." Data refer to Diamonite ceramic, Frenchtown ceramic, and sapphire. Lines are calculated from a semi-empirical formula.

There is good agreement between the Frenchtown data, the Diamonite data, and the theoretical line family previously derived, in spite of the finding that Frenchtown #4462 is incompatible with cesium. Apparently, operation of the cesium still and getter ion pump in both experiments is sufficient to maintain similar fairly clean surfaces.

d. Data After Pinchoff

Having acquired some data on a continuously gettered system, it was decided to acquire some data on an isolated, pinched-off system. Cesium was distilled into the tube of Fig. 2 (initially upside down) and then the tube

was pinched off as shown by the dashed lines in the figure. Special ovens were designed to keep T and T' at desired and independently controlled values. The purpose of the intermediate ceramic was to regulate carefully the cesium liquid level and cesium arrival rate; cesium does not wet the intermediate ceramic with a temperature greater than T'.

After a few preliminary runs, conductivity data became reproducible. This was unexpected because no getter ion pump was present to remove continually accumulated gases. In fact, readings taken three months apart with the tube kept hot gave identical results. Also after accidently heating the surface to 900°K for a few seconds, results were still identical.

Runs #7 to 14 are shown in Fig. 6. There is a definite family of sloping lines intercepting the vertical lines at about 10^{-4} mho/square in agreement with Fig. 4, but the slope in Fig. 6 is only 1/3 that of Fig. 4. The presence

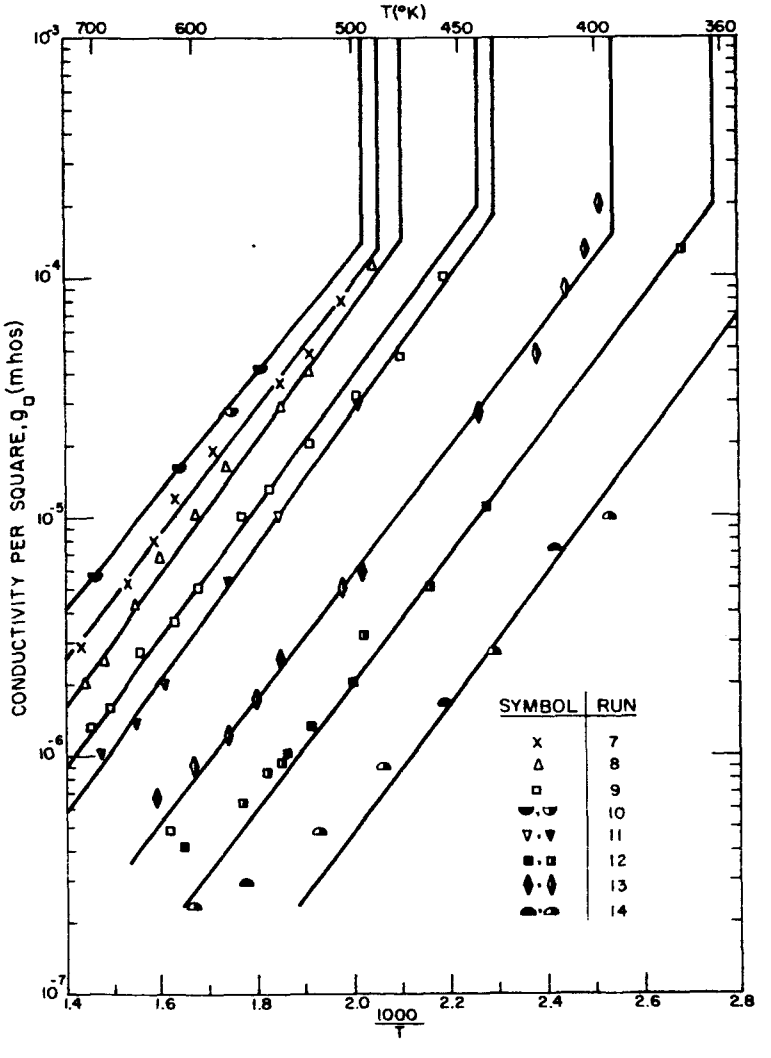

Fig. 6.
Conductivity versus reciprocal surface temperature for cesium on Frenchtown ceramic with getter ion pump off. The increase in conductivity is due to buildup of contaminant gases.

of contaminant greatly increases surface conductivity. To see if there were any time lags, some data (◒, ▼, ■, ◆, and ◓) were taken at a true steady-state equilibrium, while the other data were taken under slow ramp cooling of T. There were no time lags.

A master plot of Fig. 6 is shown in Fig. 7 where it is seen that the conductivity obeys Eq. (1), but with A, B, and C values different from Eq. (2), namely

$$A = -4.5,\ B = 2400,\ C = 2700. \tag{5}$$

The close agreement of the data in Fig. 7 to the straight-line family is attributed to a precise control of the cesium arrival rate. Such control is possible by using the intermediate insulator, as described above.

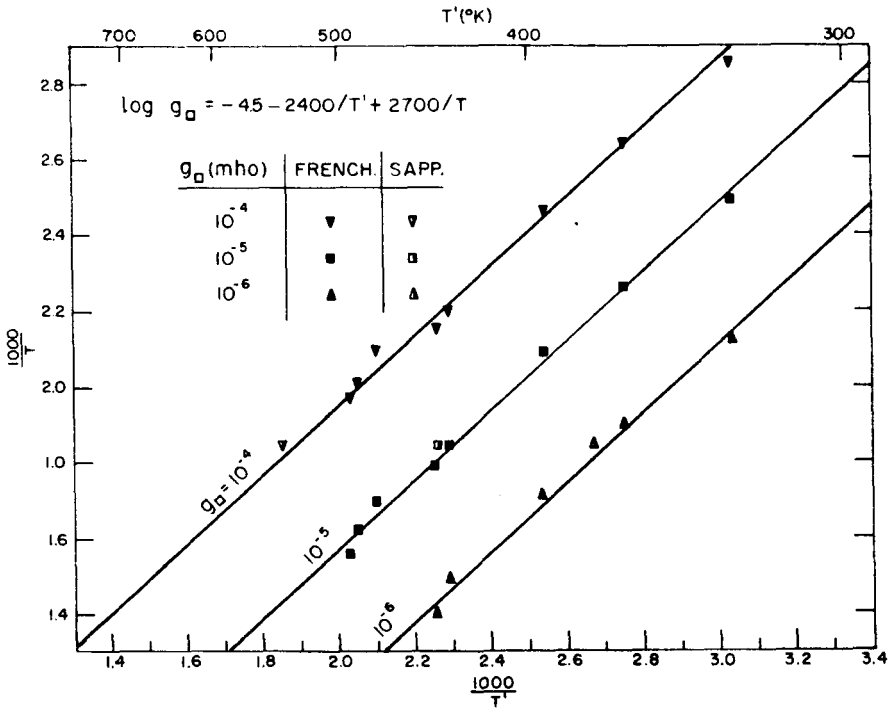

Fig. 7. Master plot of constant conductivity versus reciprocal bath and surface temperatures, taken under "unclean conditions." Data refer to Diamonite and Frenchtown ceramics. Lines are calculated from a semi-empirical formula.

e. Magnetic Field Suppression of Thermionic Emission

Shortly after pinchoff it was recognized that thermionic emission was causing curvature in the high temperature portions of the data. Therefore,

preliminary runs taken immediately after pinchoff were investigated both with and without a magnetic field of a few hundred gauss. In Fig. 8, the preliminary data points o signify no magnetic field, data points • signify magnetic field, and data points X again signify magnetic field, but data taken a day later. Initially, low thermionic emission was removed by the magnetic field, but one day after pinchoff, thermionic emission became stronger, probably due to interactions of accumulated contaminants with the metal surfaces. This could not be removed entirely by the magnetic field, and it was not possible throughout all the succeeding runs to reproduce the data points •. Instead, thermionic emission seemed to compete with surface conductivity near 10^{-6} mho/square. All runs on the Frenchtown ceramic reported in Figs. 6 and 7 were taken with the magnetic field applied.

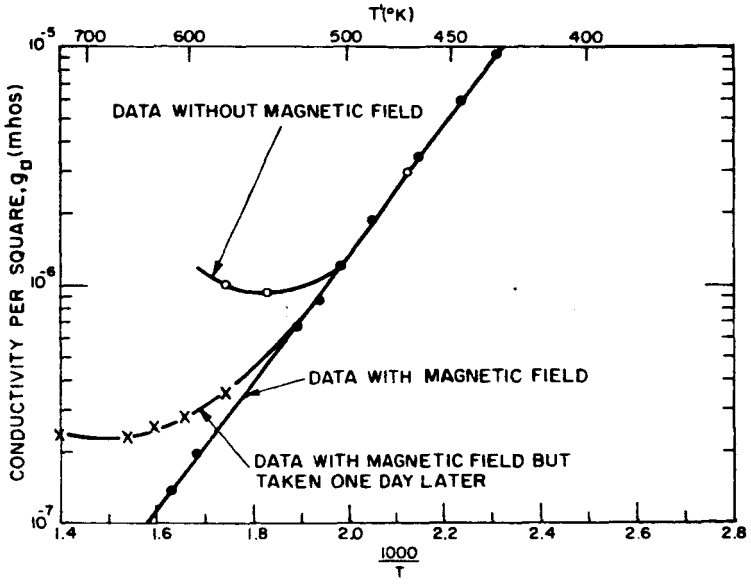

Fig. 8. Effect of magnetic field in suppressing thermionic emission. Thermionic emission builds up with time due to contaminants.

f. Ohmic Character of the Conductivity

To see if the conductivity was truly ohmic, current-voltage plots were made (3 months later), one of which is shown in Fig. 9. The data were taken by William Dennehy, a research trainee. Without a magnetic field, the data were grossly non-ohmic as shown by the points o. But with a magnetic field applied the data became ohmic over the range 0.1 to 100 volts as shown by the points •. In fact, it was later found that the data were still ohmic up to fields of 2000 volts/cm, provided measurements were made in short pulses to

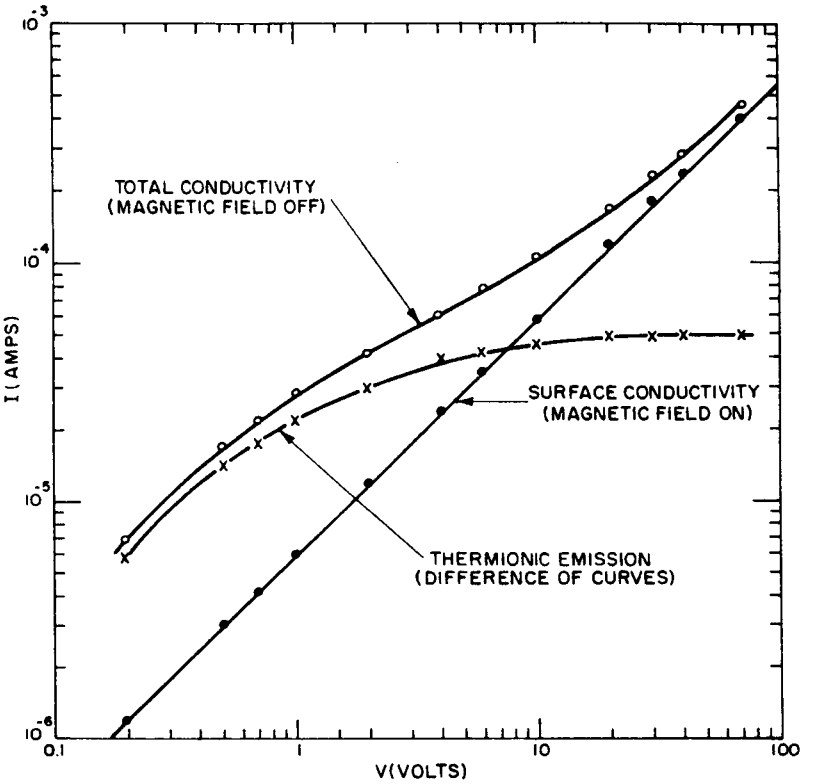

Fig. 9. I-V plot showing ohmic behavior of surface conductivity provided magnetic field is applied. The difference between measurements with and without magnetic field gives the thermionic emission characteristic.

avoid joule heating of the cesium film. The portion of the conductivity which is removed by the magnetic field is obtained by subtraction and is shown by crosses in the same figure. The resulting curve strongly resembles an I-V characteristic of thermionic emission, as originally suspected.

2. Cesium Adsorption on Sapphire

a. Experimental Arrangement

A sapphire rod of length 6 cm and diameter 0.1 cm was chosen for this experiment. The rod was chemically and ultrasonically cleaned, joined by molybdenum metallizing to Kovar cups on top and bottom, and spring-mounted in a Pyrex glass tube as shown in Fig. 10. Thermocouple leads were attached to one Kovar cup so that the sapphire temperature could be ascertained directly. The glass was chosen to be Pyrex to help avoid the "blue" problem.[19] A barium getter was flashed in the cesium reservoir and this served to trap the small amount of "blue". A separate heater ring was placed around the glass to

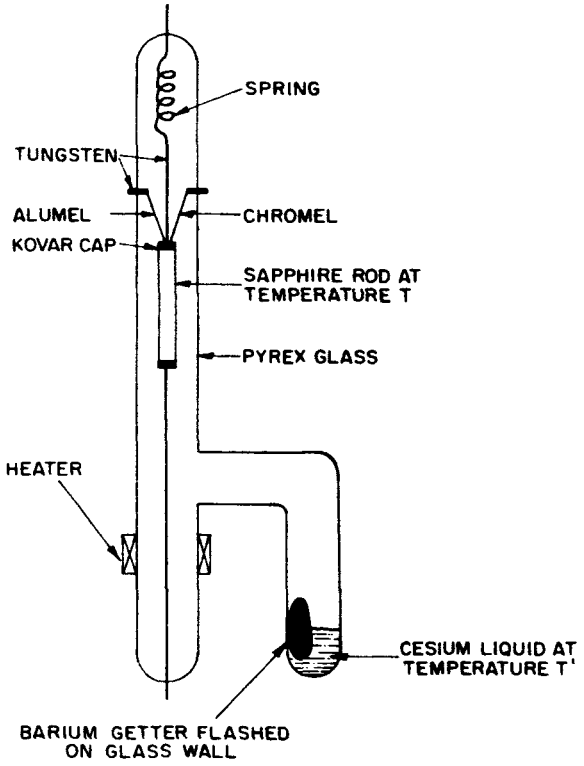

Fig. 10.
Tube used for measuring conductivity of cesium films adsorbed on sapphire. Dynamic equilibrium is established between adsorbed cesium and cesium vapor.

eliminate electrical conductance along the inner glass walls; the required temperature increase there was only about 20°C.. A large copper oven was placed over the long tube to give a constant T in the vicinity of the sapphire; a smaller copper oven was placed about the cesium reservoir to give a constant T'; and an intermediate heater was placed at the neck to keep the liquid always in the reservoir.

The tube was processed by baking out under vacuum but was tested without a getter ion pump or ion gauge. It was hoped that the barium getter would continually keep the background pressure at a low level. The inadequacy of this presumption is shown by the slow drifts in the data described below.

b. Experimental Data and Long Time Drifts

Data were taken by fixing T and continuously varying T'. This procedure happened to be more convenient than fixing T' and continuously varying T, as was done with the Frenchtown system. Typical data are shown in Fig. 11 for runs #1, 5, 18, 21, and 23.

The first few runs, #1 to 5, are taken within 4 days of starting and are very similar to the data of the continuously gettered Diamonite and Frenchtown systems, as can be seen in two ways. First, the slopes of runs #1 and #5 are

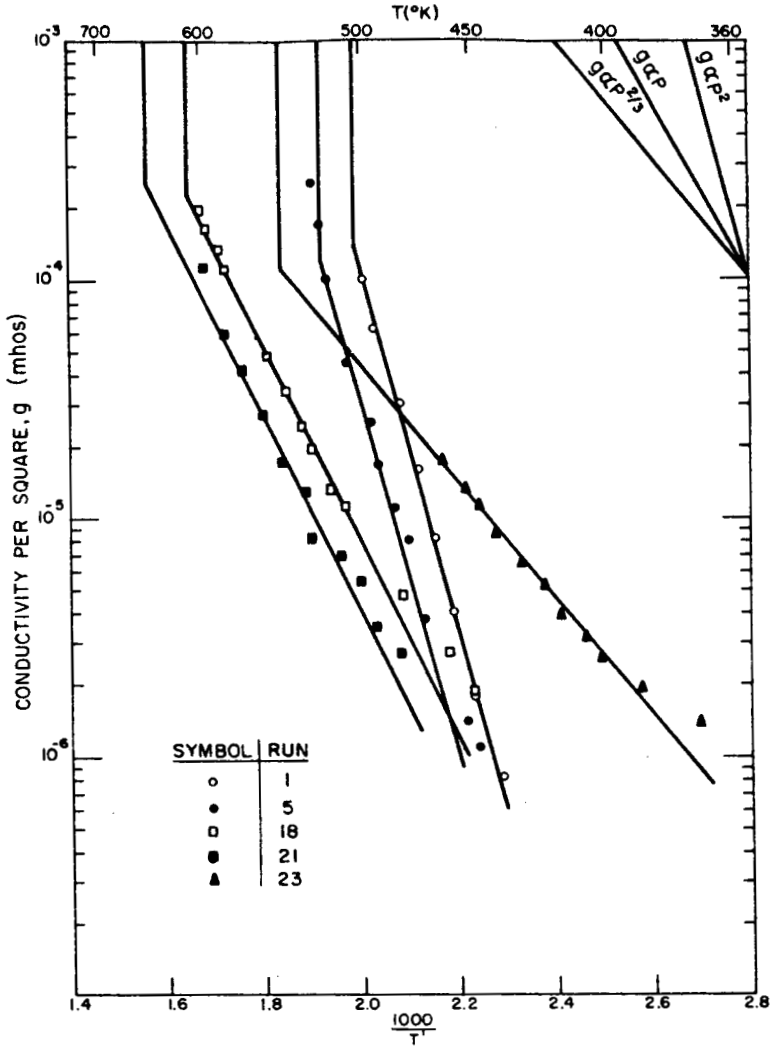

Fig. 11. Conductivity versus reciprocal bath temperature for cesium on sapphire. Increases of conductivity with time are due to buildup of contaminant gases. The insert shows theoretical proportionalities between conductivity and cesium pressure.

identical with the slope of conductivity proportional to pressure squared, as shown in the insert of Fig. 11. Second, runs #1 and #5, when plotted directly on the master chart of Fig. 5, agree well with data there.

But runs taken about one month after starting showed different behavior, as typified by runs #18 and #21 of Fig. 11. Intermediate runs #5 to #18 are not shown to avoid cluttering the figure. There was observed a definite decrease of slope with increase of time after initial startings.

The last run taken, run #23, was characteristic of the pinched-off Frenchtown ceramic system as can be shown in two ways. First, the slope of run #23

is identical to the slope of $g \propto p^{2/3}$ as shown in the insert of Fig. 11. Second, run #23 plotted directly on the master chart of Fig. 7, agrees well with the isolated Frenchtown data.

The tube failed due to an accidental overheating before it could be established whether an equilibrium was reached at the relation $g \propto p^{2/3}$.

c. Conductivity of Sapphire with Adsorbed Cesium in Presence of Air

After removing the sapphire rod with adsorbed cesium on it, and after letting it remain one day in air at room temperature, electrical conductivity measurements were made. Examples of these measurements are shown in Fig. 12. Run #2 shows a lower conductivity than run #1 because of evaporation of cesium at the high temperatures of run #1. But the ionization energy (activation

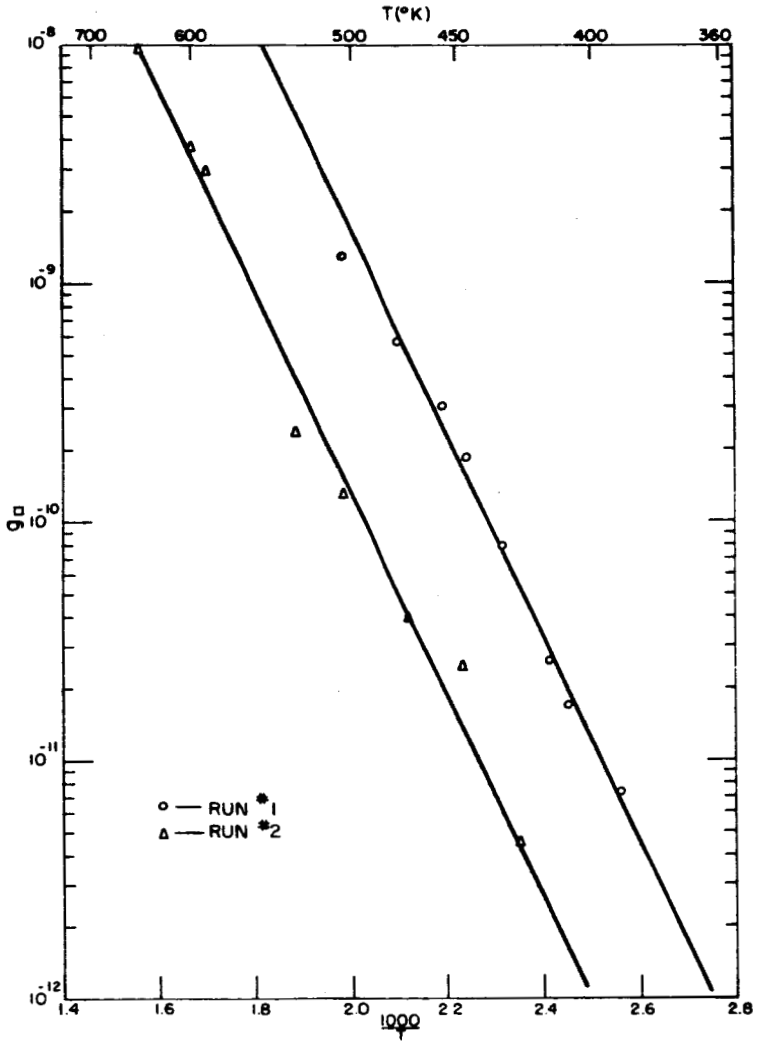

Fig. 12. Conductivity versus reciprocal surface temperature for adsorbed cesium on sapphire in the presence of air.

energy for conduction) is fairly constant for both runs and is equal to 0.87 ev. This value is in between that of pure sapphire (~1.7 ev) and that of cesium films unexposed to air (~0.05 ev as shown in Section I-D of this report); but it practically coincides with the ionization energy for Pyrex glass, so it was suspected that glass could have evaporated from the glass walls on to the sapphire surface. The following experiment showed that this is not the case.

d. Mass Spectrographic Analysis of Sapphire Rod

The sapphire rod was sent to the RCA Mass Spectrographic Laboratory where it was analyzed by sparking a part of the rod surface. The depth of the spark was estimated to be $\sim 10^{-4}$ cm within a factor of 10. Results of the analysis showed 200 ppm of cesium (resolution 10 ppm) which could be accounted for by about one monolayer of adsorbed cesium (i.e., $200 \times 10^{-6} \times 10^{22}$ bulk atoms/cm^3 $\times 10^{-4}$ cm $= 2 \times 10^{14}$ Cs atoms/cm^2 $= \sim 1$ monolayer). But no silicon was detected showing that glass had not contaminated the sapphire surface as suspected from the data in Fig. 12. It was also suspected that molybdenum from the metallizing at the rod ends could have become sufficiently mobile to contaminate the surface. But no molybdenum was detected in the mass spectrographic analysis. It was concluded that the ionization energy of 0.87 ev is probably due to monolayers of cesium oxide or cesium hydride.

3. Cesium Adsorption of Pyrex Glass

Recently, Blackford[18] reported some conductivity data for cesium on #7740 Pyrex glass in the temperature range $300°K < T, T' < 400°K$. There was no gas-purifying system. For $T > 400°K$ and $T' = 340°K$, he observed curves in his data which he could not explain, but which we now see are attributable to thermionic emission. Data of all his 4 runs are replotted onto a master chart as shown in Fig. 13.

The empirical equations which correlate his data are Eqs. (1) and (2) except that A is -6.6, instead of -5.4. In other words, the curves of Fig. 13 and Fig. 5 are simply related by a translation of about one vertical unit.

Since Blackford measured only 4 runs and operated with a very low cesium bath temperature, he probably did not observe buildup of accumulated gases reported above for closed-off systems.

Yet it is remarkable that electrical conductivity of cesium on glass and ceramic obeys a similar empirical law.

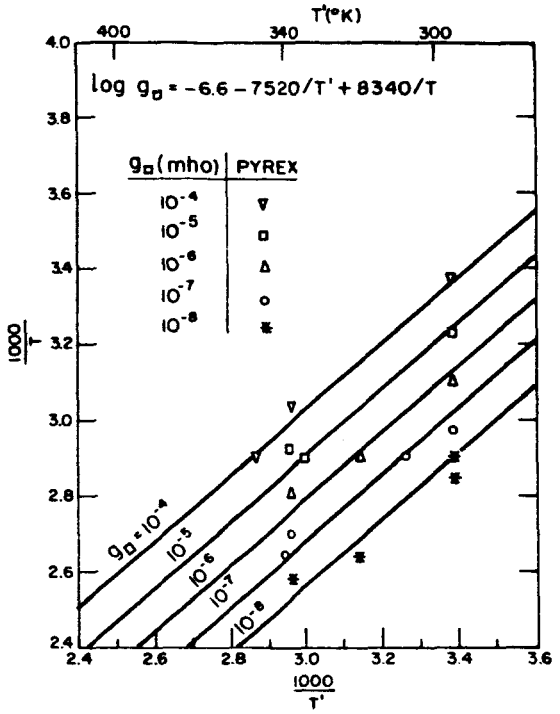

Fig. 13. Master plot of Blackford's cesium on Pyrex data. The semi-empirical line formula is similar to that of cesium on ceramic under "clean" conditions.

4. Discussion

The conductivity of insulators coated with adsorbed cesium in equilibrium with cesium vapor has been studied sufficiently to draw some broad generalizations.

For "clean" alumina ceramic or sapphire systems (defined roughly as continuously gettered systems, or closed systems in initial stages of life), conductivity is found to follow the semiempirical law

$$\log g_{\square} = -5.4 - 7520/T' + 8340/T \qquad (6)$$

This is somewhat surprising since some ceramics are compatible and others less compatible with cesium, and since sapphire is a single crystal and alumina ceramics are polycrystalline with additive binders. Apparently, conductivity is independent of the band structure or chemical character of the substrate; thus, theoretical adsorption models involving bands, band-bending, or localized chemical bonds cannot apply. Most probably, conductivity proceeds by "impurity band conduction". This term has been coined by others to describe strong interactions between donor impurities in highly doped semiconductors;

such interactions are therefore independent of the host crystal.[17,21,22] It seems that there is a close analogue between this concept of semiconductor theory and the cesium on ceramic system in interest.

A more direct evidence of cesium-cesium interactions is the proportionality of conductivity to cesium pressure squared, as seen from Eq. (6).

For "unclean" ceramic systems (defined roughly as unpurified systems in later stages of life where gas can accumulate) the conductivity is found to be much larger than for "clean" systems, and obeys a different semiempirical law. The contaminant gas is unknown, but as it accumulates, the electrical conductivity across the ceramic and the thermionic emission from adjoining metal points both increase.

C. CONDUCTANCE KINETICS DURING CONTINUOUS CESIUM DEPOSITION AT 77°K

The main objective of a conductance kinetic study is to find an empirical relation between conductivity, time of cesium deposition, and cesium arrival rate. From this relation, we can then deduce the presence of cesium traps, the order of the kinetics, and the mechanism for conduction. Careful conductance kinetics studies have been made for tin and lead films[23] and for cesium, rubidum, and potassium films[18] many monolayers thick, but no careful studies have been carried out for the monolayer range of interest. Let us first consider a very simple model which will guide interpretation of the experimental data to follow.

1. Simple Model of Conductance Kinetics

Consider an insulator surface exposed for a time t to a constant arrival rate A of cesium vapor. Then if the surface is sufficiently cold, no desorption can occur and the concentration N_1 of cesium atoms builds up as $N_1 = At$. But if there are traps with a constant concentration N_x, then the concentration of free (or untrapped) cesium atoms is

$$N_1 = A\,(t-\tau) \tag{7}$$

where τ is the trap-filling time defined by

$$N_x = A\tau. \tag{8}$$

From Sect. I-B and reference 19 there is strong reason to anticipate cooperative cesium interactions and possibly the existence of diatomic molecules on the

surface. Let us therefore continue the simple kinetic model based on the anticipation of diatomic molecule formation though this may not be the correct or the only cesium interaction.

The rate of diatomic molecule formation, at a concentration N_2, is given by

$$\frac{dN_2}{dt} = \gamma N_1^2 \tag{9}$$

where γ is a second order rate constant. Provided $N_1 \gg N_2$, the combination of Eqs. (7) and (9) yields a third order kinetic equation upon integration:

$$N_2 = \frac{\gamma}{3} A^2(t-\tau)^3. \tag{10}$$

Furthermore, if the conductivity is proportional to N_2, we have

$$g = bA^2(t-\tau)^3 \tag{11}$$

where b is another constant at a given surface temperature. A more general form of Eq. (11) is

$$g = bA^m(t-\tau)^n \tag{12}$$

where m and n are numbers to be determined from experiment, and to be compared with theoretical values of 2 and 3, respectively.

This model shows that if $m = 1$ and $n = 1$, single cesium atoms individually contribute to conductivity; but if m and n are larger integers, then diatomic molecules or possibly larger aggregates contribute to conductivity. The data to follow shows that $m = n = 4$. One weakness of the model is its neglect of lateral cesium diffusion which is considerable at conductances higher than about 10^{-6} mho as seen in Section I-E.

2. Experimental Arrangement

A schematic diagram of the cesium deposition apparatus designed by J. Fendley, Jr., is shown in Fig. 14. The cesium in a copper reservoir is designed to escape through a pinhole at a rate controlled by the reservoir temperature (nominally 373°K). A sliding shutter operated by a bellows allows the thermal cesium beam to be easily turned on or off. The walls between the reservoir and the target are kept at 77°K by liquid nitrogen poured into an internal tank; this serves to trap cesium that arrives there (vaporization rate for bulk cesium extrapolated to 77°K is 10^{-24} atoms/cm^{2}sec). The cesium beam arrives at the sapphire disc, becomes adsorbed there and increases the conductivity. The disc

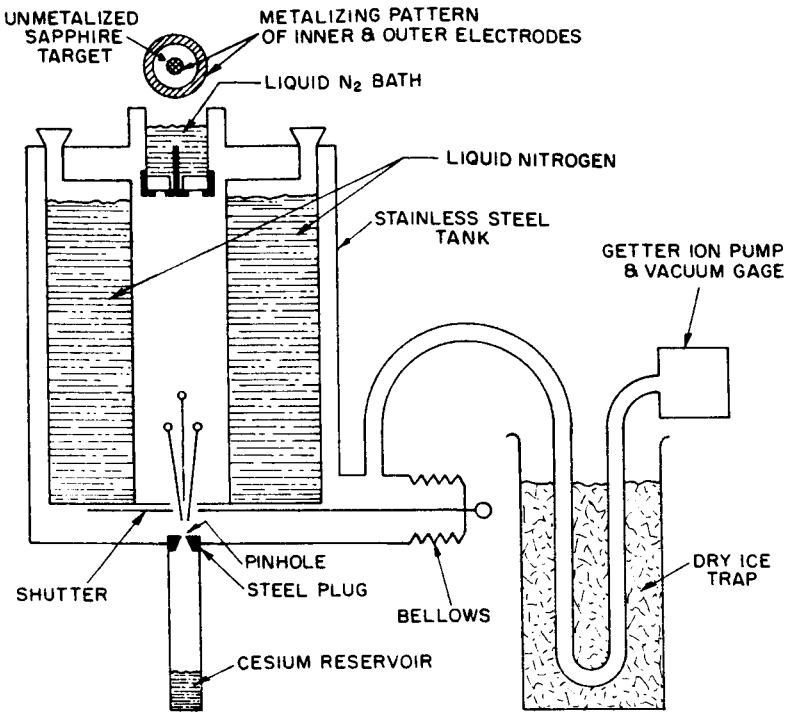

Fig. 14. Schematic experimental arrangement for depositing controlled amounts of cesium on a cold sapphire target. Conductivity across the sapphire proceeds radially via the deposited cesium film.

is metallized on inside and outside so that the path of electrical conductivity is radial. A Kovar pin attached to the center metallizing provides the inner electrical connection. Liquid nitrogen can be poured into the well above the sapphire to insure a constant disc temperature of 77°K. Finally a getter ion pump and an ion gauge is attached through a dry ice trap. During the runs, there was no gauge deflection, so the background pressure was definitely less than 10^{-8} Torr, and probably about 10^{-12} Torr due to the chemical gettering action of cesium continuously deposited on large area walls at 77°K.[23]

The main philosophy in designing the apparatus is to insure cesium compatibility (stainless steel, copper, and Kovar parts) and demountability. The apparatus is versatile: other targets besides sapphire can easily be used.

3. Experimental Procedure

The procedure in taking a typical run is as follows.

a. Fix desired reservoir temperature T'. The arrival rate, A, at the target can be calculated from

$$A = A' r_p^2 L^{-2} = 0.95 \times 10^{-5} A' \text{ (atoms/cm}^2 \text{ sec)} \qquad (13)$$

where A' is the arrival rate at the pinhole of radius r_p, and L is the distance from pinhole to target. The geometry correction factor is $(0.0247"/8")^2$ or 0.95×10^{-5}. No independent arrival rate calibrator was used.

b. Open shutter and allow cesium to arrive on sapphire target precooled to 77°K.

c. Monitor the conductivity g versus time after opening shutter. This is done most easily by connecting a Keithley 610 ohmmeter directly to an X-Y time base recorder. If desired, the conductivity per square $g_\square$ can be calculated from the inner radius $r_1 = 0.48$ cm and the outer radius $r_2 = 0.96$ cm, from the relation

$$g_\square = g\ 2\pi\ [\ln(r_2/r_1)]^{-1} = 0.110\ g \qquad (14)$$

d. At end of run, close shutter.

e. To start another run, warm target to ~75°C by using a hot air blower together with a funnel. The liquid nitrogen pool is rapidly removed this way and the sapphire can be directly warmed, still keeping the supporting massive stainless steel parts cold. Heating of the sapphire is stopped when condensed water evaporates from the warmed sapphire. This procedure is found sufficient to drive away all the cesium present on the sapphire.

f. Pour liquid nitrogen back in the target well. Fortunately, the sapphire to Kovar metallizing can withstand the sudden thermal shock. The time to warm and cool is only about five minutes.

g. Take a new run by repeating (b), or else change reservoir temperature and then repeat (b).

As a variation, sometimes the conductivity is monitored <u>after</u> the shutter is closed. This variation will be discussed in Section I-E.

The procedures above are especially simple when compared to those used by Appleyard and Lovell. They used a Pyrex glass target and found it necessary to prewarm the target to 200°C for an hour before their runs could be reproducible. The problems of chemical reaction are serious under such conditions. We require, by contrast, a warming to only about 75°C and waiting only 5 minutes before reproducible runs can be obtained. Furthermore, cesium is known not to chemically attack sapphire (100% single crystal Al_2O_3).

4. Kinetic Data

Some examples of runs taken with the above procedure are shown in Fig. 15. In all these runs, the cesium reservoir is immersed in boiling water (373°K). But because there is no precise control on the water level due to bubbling and evaporation, it is estimated that the temperature near the pinhole may have fluctuated by about 3°C. The runs show the following pattern. For times less than about 200 seconds after opening the shutter there is no evidence of conductivity. Suddenly, conductivity appears and rises rapidly with time but then rises less rapidly. There is no evidence of saturation. The runs are stopped by closing the shutter at various times shown by the arrows in the figure. For conductivities $>10^{-9}$ mho the conductivity always decays with time. This phenomenon is shown in Section I-E to be due to lateral diffusion. All these qualitative results were reported first in the pioneering studies of Appleyard and Lovell, but they did not study the phenomena in depth because they were more interested in thicker films of the order of 100 Å - 1000 Å.

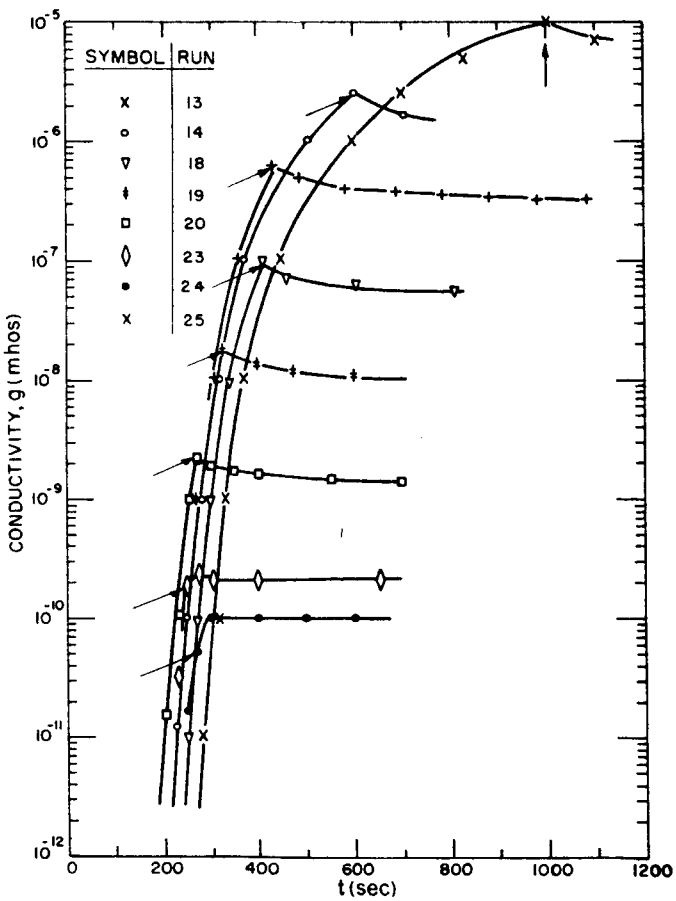

Fig. 15.
Conductivity at 77°K versus time after opening shutter with T′ = 373°K. Arrows point to closing of shutter followed by conductivity drifts. Data is fairly reproducible.

The data of Fig. 15 shows that the system is fairly reproducible. As previously mentioned, part of the scatter may be due to imperfect temperature control.

To show the great sensitivity of conductivity data to reservoir temperature, other runs shown in Fig. 16 were taken with an electrical reservoir heater. Variations of 30° reservoir temperature are sufficient to vary the conductivity by as much as 6 orders in magnitude at constant deposition time. But the data will be more informative if it can be cast in the form of Eq. (12), so that the parameters τ, m, n, and b can be calculated.

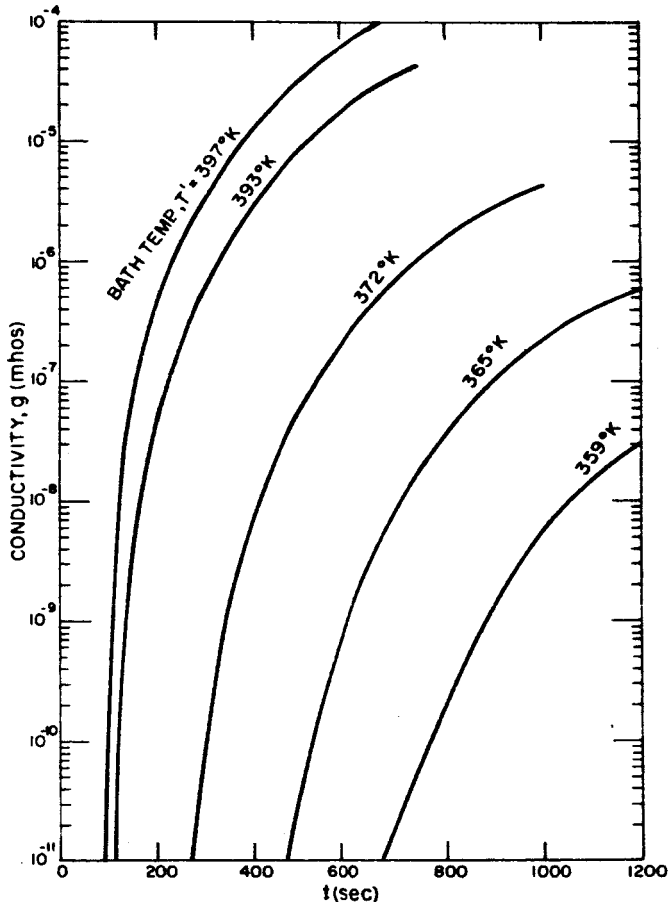

Fig. 16. Strong dependence of conductivity on bath temperature.

a. Calculation of τ and N_x

τ can be determined from conductivity data by experimentally measuring the slope S of Eq. (11) and the time t when the conductivity is 10^{-11} mho,

then

$$S_{11} \equiv \frac{d \log g_{11}}{dt} = \frac{3}{2.3(t_{11}-\tau)} \cdot \qquad (15)$$

Values of t_{11} (time to reach 10^{-11} mho) are shown for some runs in Table I. A rearrangement of Eq. (15) yields

$$\tau = t_{11} - 1.3/S_{11} \qquad (16)$$

from which τ can be calculated as also shown in Table I. Note that τ is ~90% of t_{11} and so is not greatly altered if the exponent m differs from the expected value of 3. Finally the product $N_x = A\tau$ can be calculated and is also shown in the Table. N_x is $\sim 2.5 \times 10^{14}$ traps/cm^2 and is independent of arrival rate variations over two orders in magnitude. The numerical magnitude of N_x indicates

TABLE I

INSENSITIVITY OF CESIUM TRAP DENSITY(N_x)
TO CESIUM ARRIVAL RATE(A)

T' (°K)	Run	A (#/cm^2 sec) x 10^{11}	t_{11} (sec)	τ (sec)	$N_x = A\tau$ (traps/cm^2) x 10^{14}
350	39	1.9	1330	1030	1.8
359	32	3.4	725	615	2.0
365	33	5.0	480	415	2.0
372	30	7.8	285	256	1.9
374	38	9.0	295	250	2.1
383	37	15.	203	185	2.6
393	28	27.	120	94	2.4
397	29	34.	95	90	2.9
403	34	46.	60	54	2.4
403	35	46.	71	64	2.8
414	40	81.	60	57	4.4
421	41	170.	20	17	2.7
Mean cesium trap density is $N_x = 2.5 \pm 0.7 \times 10^{14}$ cesium traps/cm^2					

that the first 1/2 monolayer of deposited cesium is electrically inert in quantitative agreement with Appleyard and Lovell. The constancy of N_x is in agreement with the presumption made in Eq. (8).

b. Calculation of n

The quantity n can be determined by plotting log g versus log $(t-\tau)$ for the various constant arrival rates of Table I, as shown in Fig. 17. The slope of the line family on this plot is n, which is found to be ≈ 4 by comparison with the insert. For conductivities $g > 10^{-6}$ mho, the slope is smaller and $n \approx 3$.

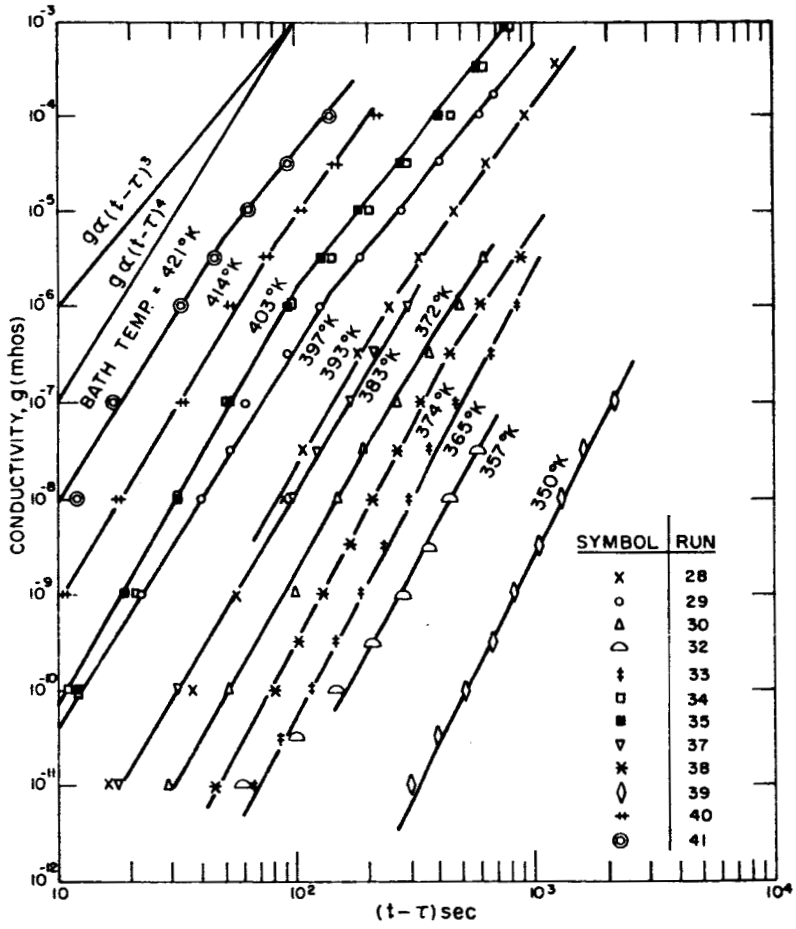

Fig. 17. Log conductivity at 77°K versus log $(t-\tau)$ at various constant arrival rates. By comparing data with theoretical slopes in the insert, the experimental slope, n, is about 4.

c. Calculation of m

The quantity m can be determined most easily by connecting points of constant $(t-\tau)$ from Fig. 17, as shown in Fig. 18. Here log g is plotted versus

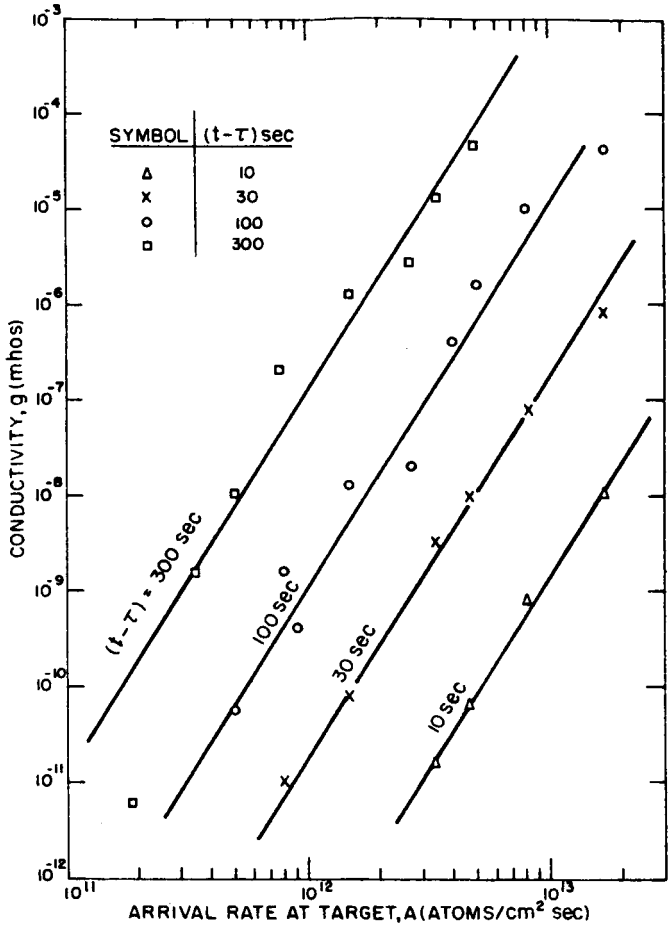

Fig. 18. Log conductivity at 77°K versus log arrival rate at various constant values of (t-τ). The experimental slope, m, is 4.

log A for (t-τ) held constant at 10, 30, 100, and 300 sec. The slope of the line family on this plot is m. In fact, the choice of m = 4 passes through all the data.

d. Calculation of b

The quantity b can be calculated from spot checks of Fig. 18, using Eq. (12) and m = n = 4. Various log b values are found to be -65, -64, -64, and -65, giving an average of -64.5. The dimensions of b are cm^8 mho.

5. Discussion of Conductivity Kinetics

Summing the results of the calculations above, the conductivity per square at 77°K is found to be accurately described by the semiempirical formulas

$$g_{\square} = 3.5 \times 10^{-66} A^4 (t-\tau)^4 \text{ mho} \qquad (17)$$

$$\tau = 2.5 \times 10^{14}/A \text{ sec} \qquad (17a)$$

Eqs. (17) and (17a) have been found to apply at T = 77°K for $10^{-12} < g_{\square} < 10^{-4}$ mho, $10^{11} < A < 10^{13}$ atoms $cm^{-2}sec^{-1}$ and $10 < t < 1000$ sec. Studies outside this range have not been attempted. In particular, the coefficient of Eq. (17) may depend strongly on surface temperature which is here held fixed at 77°K.

The high fourth power kinetic order of the equation definitely points to cesium-cesium interactions required to form a conducting cesium species. Such interactions are consistent with our previous interpretations of dynamic equilibrium data in Section I-B.

The constancy of the trap concentration $N_x = A\tau$ definitely shows that the first half layer of absorbed cesium on insulations is electrically inert at 77°K.

D. ACTIVATION ENERGY FOR CONDUCTION

Conductivity of ultra-thin films may usually be expressed by

$$g = g_i e^{-\epsilon_i/kT} \tag{18}$$

where g_i is an "initial conductivity (a function of cesium coverage but not temperature), ϵ_i is the corresponding activation energy for conduction (also a function of coverage but not temperature), k is Boltzmann's constant, and T is the surface temperature. The quantity ϵ_i is frequently called the "ionization energy" following usual semiconductor terminology,[24] but ϵ_i is less than 0.01 ev, and is not directly related to the much greater ionization energy of a free cesium atom in the vapor state.

The parameters ϵ_i and g_i can give important clues to understanding cesium-cesium interactions.[25]

Measurements of ϵ_i and g_i have been made with the continuous cesium deposition apparatus described in Sect. I-C. The experimental technique consists of immersing the sapphire target in liquid oxygen (90°K), then in liquid nitrogen (77°K), and finally back in liquid oxygen to check for reproducibility. Data taken in this way is shown in Fig. 19, where log g is plotted versus 1000/T. Lines are drawn through the corresponding points of a run; these points are fairly reproducible, but drifted slightly downwards with time due to slow diffusion as described in Section I-E. The pattern emerging from this family of data is similar to that found by Neugebauer[14] for platinum films, Feldman[26]

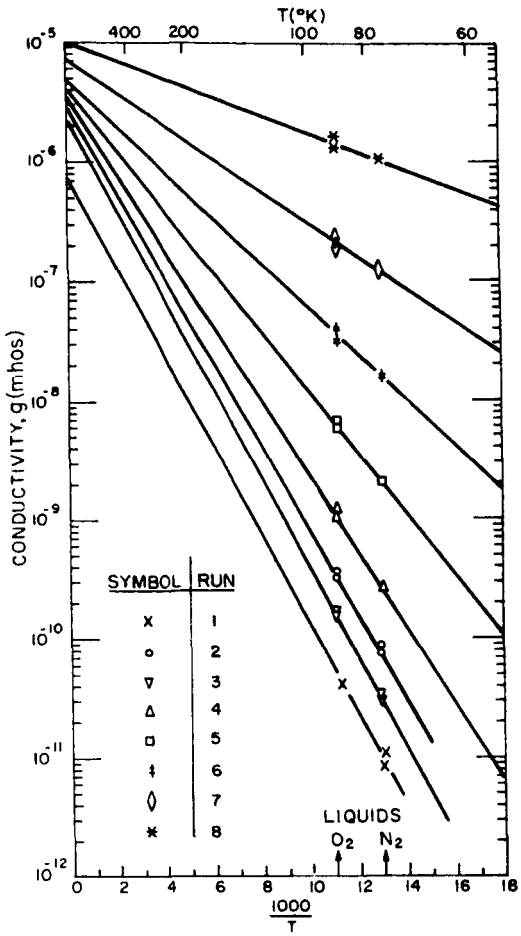

Fig. 19.
Conductivity versus reciprocal sapphire temperature. Lines correspond to constant coverage; slopes give ionization energy for conduction, and intercepts give "initial" conductivity.

for platinum and gold films, and Wei[27] for potassium films. But the data in Fig. 19 cover a larger range of conductivities; i.e., from 10^{-11} to 10^{-6} mho.

From the line slopes in Fig. 19, ϵ_i can be calculated; and from the line intercepts, g_i and the initial conductivity per square, $g_{i\square} = 0.110\ g_i$ can also be calculated. An illuminating cross plot of ϵ_i versus $g_{i\square}$ is shown in Fig. 20. For $g_{i\square} < 2 \times 10^{-8}$ mho, ϵ_i is a constant = 0.076 ev, showing lack of lateral interactions at extremely low coverages. But as coverage and $g_{i\square}$ both increase, cesium-cesium interactions cause ϵ_i to be lowered. Finally, for $g_{i\square} > 7 \times 10^{-7}$, ϵ_i is less than thermal energy, kT, at room temperature.

One can predict from this data (taken at cryogenic temperatures) that for temperatures > 300°K, a system with a measured conductivity > 10^{-6} mho has $\epsilon_i > kT$, and therefore essentially consists of ionized cesium. It is gratifying to note that the concept of ionized cesium on insulators was first presumed without proof in reference 19. The nature of cesium interactions will be considered in more detail and will be reported at a later date.

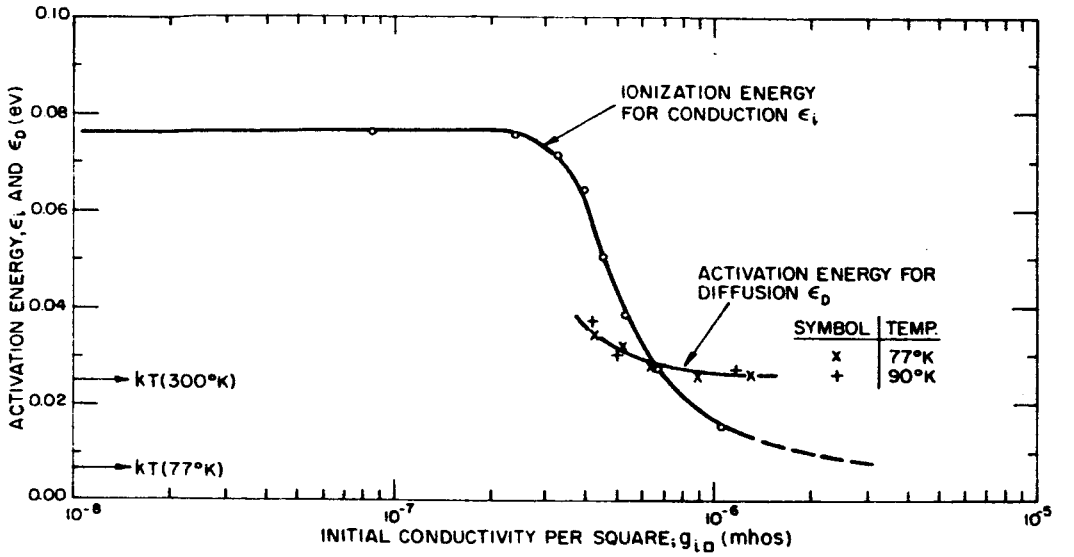

Fig. 20. Change in conductivity versus time after closing shutter at 77°K and 90°K. Each line corresponds to a different conductivity at the instant of closing the shutter. All data follow the 1/2 power law characteristic of diffusion processes.

E. CESIUM SURFACE DIFFUSION

In investigating conductivity kinetics (Section I-C), it was found that after shutting off the cesium atomic beam the conductivity drifts with time. These drifts are seen clearly in Fig. 15 where the arrows point to the rapid insertion of the shutter (only 2 seconds to close).

In general, the drifts have the following behavior. If the conductivity g_s (conductivity at close of shutter) is less than 10^{-9} mho, conductivity first increases with time. This increase has been reproduced many times at 77°K, 90°K, and 198°K, and it may be due to cesium atoms diffusing and combining to form diatomic or other aggregates which can conduct.

On the other hand, if g_s is greater than 10^{-9} mho, conductivity always decreases with time. Eventually the drifts seem to vanish, but drifts of a few percent per hour still remain. Similar conductivity decays are reported by Appleyard and Lovell. Conductivity decays may be attributed to diffusion of conductivity cesium species from the insulator surface to the metal electrode where they are presumed more tightly bound; this concept will be cast into a theoretical model and compared with comprehensive experiment data to follow.

1. Theoretical Model of Diffusion to Electrodes

To derive an appropriate equation needed for interpreting the data to follow, consider the following idealized assumptions:

a. Conductivity is proportional to the conducting species of cesium present (possibly diatomic molecules).

b. Change in conductivity after closing the shutter is proportional to the conducting species of cesium which has diffused irreversibly to the metal electrodes (where stronger binding is presumed).

c. At the time of shutting off the atomic beam, the conducting species of cesium is uniformly distributed over the sapphire surface.

It then follows from simple diffusion theory[28] in the limit of small times that

$$\Delta g = g_s \frac{(\text{circumference})}{(\text{area})} \left(\frac{4\ Dt}{\pi}\right)^{1/2} \tag{19}$$

$$= 4.8\ g_s\ D^{1/2} t^{1/2} \tag{20}$$

Here g_s and Δg are respectively the conductivity at closing of the shutter and the subsequent change in conductivity in mho units; the circumference of the electrodes is 9.0 cm; the area of the unmetallized sapphire is 2.1 cm^2; D is expressed in cm^2/sec units; and t is expressed in seconds. Note that both g_s and Δg have strong temperature coefficients of the form

$$g_s = g_{si} e^{-\epsilon_i/kT} \tag{21}$$

$$\Delta g = \Delta g_i e^{-\epsilon_i/kT} \tag{22}$$

but they effectively cancel out when solving for the diffusion coefficient D in Eq. (19). Furthermore, D is theoretically expected to have a separate temperature coefficient of the form

$$D = \ell^2\ \nu \exp(-\epsilon_D/kT) = 2.2 \times 10^{-3} \exp(-\epsilon_D/kT) \tag{23}$$

where ϵ_D is an activation energy for diffusion; ℓ is a hopping distance taken to be one cesium diameter = 4.70×10^{-8} cm, and ν is a lateral vibration frequency taken to be 10^{12} sec^{-1}. These theoretical concepts will be compared with experimental data below. Although the one-half power law of Eq. (23) has been applied to detect diffusion in other systems, such as gas diffusion in metals,[29] the law has not been applied before to conductivity of surface films.

2. Diffusion Data

Families of diffusion data arranged in the form of Eq. (20) are shown in Fig. 21 for T fixed at 77°K and 90°K. The ordinate is log Δg, the abcissa is log t, and the straight lines drawn through data points have the theoretically predicted slope of 1/2. In Fig. 21 the seven sets of data at 77°K are taken

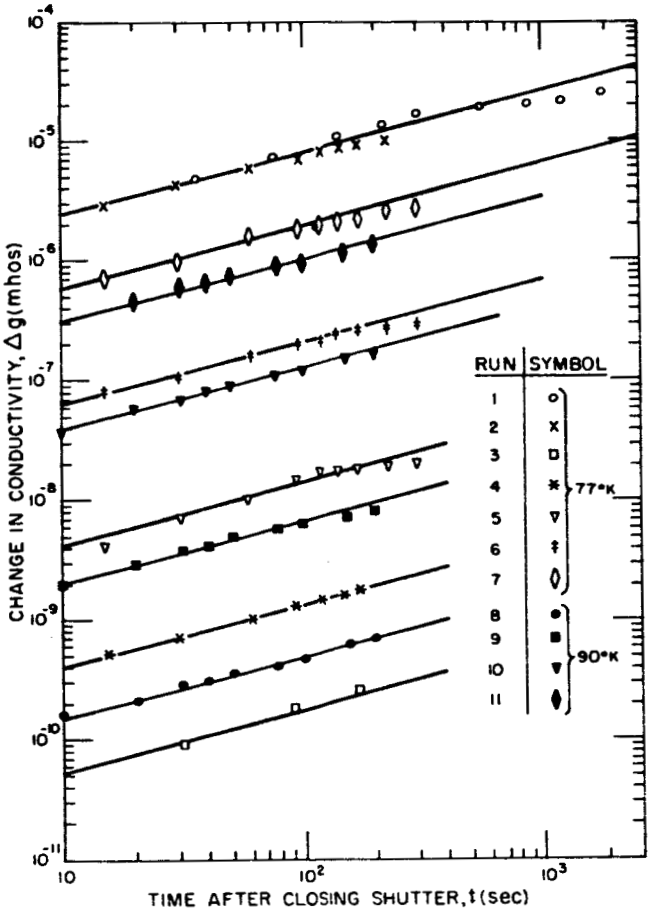

Fig. 21. Ionization energy for conduction and activation energy for diffusion versus initial conductivity per square. The decrease in these energies is due to cesium-cesium interactions at high cesium concentrations.

with $10^{-10} < g_s < 10^{-5}$ mho, while the 4 sets of data at 90°K are taken with $10^{-9} < g_s < 10^{-6}$ mho. In all cases, the data agree well with the theoretical slope of 1/2 as long as $0 < t < 200$ sec. For greater times, the slope seems to be smaller, but Eq. (20) is only expected to hold in the limit of small times.

The data in these figures definitely verifies the model that diffusion is causing the conductivity decays. If the decay were due to desorption then the

conductivity would decrease exponentially with time, which is not observed. Also, if the decay were due to arrival from contaminant residual gases, then there would be a greater effect of these gases at lower conductivities, which is not observed.

From the data in Fig. 21, D and ϵ_D can be calculated as shown in Table II. For all data, D lies in the range (1.2 - 7.3) x 10^{-5} cm^2sec^{-1}; and ϵ_D lies in the range 0.025 to 0.037 ev. Thus, to a first approximation ϵ_D seems independent of coverage or temperature. The observed magnitude of ϵ_D is in good agreement with the empirical law of Learn and Spriggs[30]: ϵ_D = (vaporization heat of bulk adsorbate)/28 or 0.8 ev/28 = 0.03 ev.

TABLE II

TABULATION OF DIFFUSION COEFFICIENTS AND ACTIVATION ENERGIES

Run	Temp (°K)	$g_s(T)$ (mho)	$g_{si} \times 10^6$ (mho)	$g_{si} \times 10^7$ (mho)	$D \times 10^5$ (cm^2/sec)	ϵ_D (ev)
1	77	2.9×10^{-5}	-	-	4.8	.025
2	77	2.1×10^{-5}	-	-	4.8	.026
3	77	1.0×10^{-10}	4.0	4.2	1.2	.034
4	77	5.0×10^{-9}	4.8	5.1	1.9	.032
5	77	4.7×10^{-8}	6.0	6.3	3.1	.028
6	77	5.3×10^{-7}	8.5	9.0	4.8	.025
7	77	5.0×10^{-6}	12.0	13.0	4.5	.026
8	90	2.0×10^{-9}	4.0	4.2	2.1	.037
9	90	1.9×10^{-8}	4.7	5.0	4.6	.030
10	90	3.1×10^{-7}	8.0	8.5	6.8	.027
11	90	2.4×10^{-6}	11.0	11.8	7.3	.027

But in fact ϵ_D is a weak function of cesium coverage. This can best be seen by converting g_s to g_i (using Fig. 19) and then converting g_i to $g_{i\square}$ by multiplying by 0.110, as shown in Table II. An illustrative cross-plot of ϵ_D versus $g_{i\square}$ is shown in Fig. 20. ϵ_D, like ϵ_i, decreases monotonically with $g_{i\square}$ (related to coverage), and the decrease is again presumed due to cesium interactions. Also, ϵ_D values at fixed $g_{i\square}$ are independent of temperature, as presumed in the initial derivation, so the theory is self-consistent.

To summarize, an analysis of the conductivity decay with time has shown that the one-half-power diffusion law is obeyed and that meaningful calculations can be made of the diffusion coefficient, diffusion activation energy, and their dependences on cesium coverage.

But other interpretations may be considered. For example, presume Eq. (19) to hold, but presume that atoms diffuse to and are trapped in combination with other atoms, instead of at the electrodes. Then the area-to-circumference ratio of Eq. (19) will be of atomic dimensions, say 10^{-7} cm^2sec^{-1}; and the activation energies of Table II would be increased to about 0.2 ev. But 0.2 ev is an order of magnitude greater than expected from Learn and Spriggs' empirical correlation, established for thin films of Pb, Sn, Cu, and Hg. Also, it is doubtful if a macroscopic diffusion equation such as Eq. (19) can be applied meaningfully on a microscopic scale.

F. OTHER CESIUM ON INSULATOR EXPERIMENTS

A great variety of experiments were made to help elucidate the cesium-insulator adsorption system. Those that were carried out in great detail over a large range of parameters have already been reported in Sections I-B to I-E. Other experiments were also carried out but to a lesser extent.

These cannot stand alone; but together with the more detailed studies, they help to give a comprehensive picture.

1. Thermoelectric Effect

Thermoelectric measurements made with adsorbed cesium films on ceramic and two samples of Pyrex glass show that the absolute thermoelectric power Q in the temperature range 77°K to 350°K is $0 < |Q| < 20$ microvolts/°K. Q is usually in between that of bulk cesium and that of ordinary n-type semiconductors. A parametric study of Q would be extremely useful, because its atomic interpretation[31,32] gives independent insight into the conduction mechanisms. But such a study was not carried out because of difficulties in maintaining uniform coverage and known small temperature differences, and difficulties in avoiding stray voltage sources. A new tube will be designed to eliminate such difficulties and to provide a comprehensive map of Q as a function of conductivity and temperature.

2. Hall Effect

An experiment designed to measure the Hall angle (equal to Hall voltage divided by applied voltage) was unsuccessful. Measurements for various temperatures and conductivities were drowned in uncontrollable noise so only an upper limit of the Hall angle could be estimated; this was about $\alpha = 2 \times 10^{-5}$ with B = 3000 gauss. Using Eq. (21) of reference 19, this angle corresponds to an upper limit on the electron mobility of 1.5 cm^2/volt sec. But this limit is questionable because the Hall probes were not flush with the conducting surface, and because of the unconventional cylindrical geometry used and unconventional thinness of the conducting cesium film.

3. Lack of Ionic Conduction

To show conclusively that conduction is not caused by cesium ions, a special experiment was performed. A ceramic and metal tube (previously built for another purpose) contained ~1/2 gram of cesium which was forced downwards to the reservoir by heating. Then the entire tube was immersed in liquid nitrogen to "freeze in" the cesium. Finally, a voltage was applied across the ceramic insulator in the tube in such a sense as to draw cesium positive ions (if they were the conducting species) from the top to the bottom of the insulator. Typical conditions of the experiment at 77°K were: V = 230 volts D.C., R = 6000 ohms, and I = 0.04 ampere. If ions would be transported off the insulator and not resupplied, then conductivity should drop sharply with time which was not observed. Also, if ions were transported from top to bottom but were continually supplied at the top by a few residual cesium monolayers there, then after these monolayers were depleted, the conductivity should drop sharply, but at a later time. This was not observed though the test ran six hours, which was sufficient to deplete 10^7 monolayers. There is no ionic conduction; it is purely electronic.

4. Pulse Experiments

High voltage pulse experiments were carried out at 77°K to see if a time lag was necessary to establish constant conductivity. Typical pulse conditions were: 100-volt pulse height, 20-μsec pulse width, 0.1-μsec rise time, and 100-cps repetition rate. Within the limit of detection, which was about 0.1 μsec, it was found that current exactly followed the voltage pulse; there were no time lags.

G. CONCLUSIONS DRAWN FROM THE CESIUM-ON-INSULATOR SYSTEM

The main conclusions to be drawn from the preceding six sections are:

1. For "clean" ceramic systems (defined roughly as continuously gettered systems, or closed systems in initial stages of life) conductivity of adsorbed cesium in equilibrium with cesium vapor follows the semiempirical law

$$\log g_{\square} = -5.4 - 7520/T' + 8340/T \qquad (6)$$

Conductivity varies as cesium pressure squared, at fixed ceramic temperature.

2. For "unclean" ceramic systems (defined roughly as closed systems in later stages of life where gases can accumulate) conductivity is larger and obeys a different semiempirical law. The unknown contaminant gas also serves to enhance thermionic emission.

3. The first half monolayer of cesium deposited on sapphire at 77°K is electrically inert.

4. Conductivity kinetics of cesium film deposition at 77°K obey the semiempirical laws

$$g_{\square} = 3.5 \times 10^{-66} A^4 (t-\tau)^4 \text{ mho} \qquad (17)$$

$$\tau = 2.5 \times 10^{14}/A \text{ sec} \qquad (17a)$$

5. Conductivity at constant coverage has a temperature dependence of the form

$$g = g_i e^{-\epsilon_i/kT} \qquad (18)$$

ϵ_i decreases from 0.06 ev to 0.01 ev with increasing g_i.

6. Conductivity drifts after closing shutter follow the diffusion laws

$$\Delta g = 4.8\, g_s\, D^{1/2}\, t^{1/2} \qquad (20)$$

$$D = \ell^2\, \nu \exp(-\epsilon_D/kT) \qquad (23)$$

from which the diffusion coefficient and the diffusion activation energy can be calculated. D varies from 10^{-5} to 7×10^{-5} $cm^2 sec^{-1}$ at 77°K and ϵ_D varies from 0.025 to .037 ev, depending on coverage.

7. One unifying thread connecting these somewhat scattered results is the effect of cesium-cesium interactions. These interactions cause conductivity in dynamic equilibrium to vary as pressure squared, cause conductivity kinetics to be of fourth order, and cause ϵ_i and ϵ_D to decrease with increasing coverage.

8. A second unifying thread is the nature of the conduction mechanism. Because data are insensitive to substrate insulator, one concludes that the conduction mechanism probably proceeds via an "impurity band" due to weak overlap of adsorbed cesium wave functions. Conventional band-bending concepts cannot apply.

9. A third unifying thread is the search for new experimental techniques in adsorption studies. For example, adsorption data have not (to our knowledge) been presented in the comprehensive forms of Eqs. (6), (17), or (20). Also, a thermoelectric analysis of monolayer adsorbed films, to be completed later, has not been attempted by others.

10. In the future, more quantitative statements will be made concerning cesium interactions, conduction mechanism, and binding mechanism.

II. THE EFFECTS OF PLASMA PHENOMENA ON THE V-I CHARACTERISTIC OF THE ARC MODE THERMIONIC CONVERTER

A. INTRODUCTION

The output voltage V of an arc mode cesium vapor thermionic energy converter can be written[33]

$$V = \phi_{ceff} - \phi_A - V_d \tag{24}$$

where

ϕ_A = anode work function

V_d = arc drop

ϕ_{ceff} = effective cathode work function.

For currents less than the saturated cathode emission current

$$\phi_{ceff} = \frac{kT_c}{e} \ln \frac{120\ A\ T_c^2}{I_c} \tag{25}$$

where

k = Boltzman constant

e = electronic charge

T_c = cathode temperature

A = effective cathode area

I_c = cathode emission current density.

For this discussion it will be assumed that $I_c \approx$ terminal current I. If the arc drop V_d were current-independent the volt-ampere characteristic plotted as log I versus V would be a straight line over the range of validity of Eq. (25). The slope of the line would be determined by the cathode temperature. As the saturated emission current is reached, the current would remain at a constant value independent of V. There is no experimental evidence indicating that the surface properties of the electrodes change during the recording of a volt-ampere characteristic, provided the electrode temperatures remain constant. The volt-ampere characteristic then reflects the plasma properties of the diode. If the anode work function ϕ_A is known (for instance by assuring a complete cesium film coverage of the anode) the volt-ampere

characteristic allows evaluation of the arc drop V_d which is determined by the power loss in the plasma. In general, V_d is not current-independent. The different factors influencing V_d are discussed in this section. Another current-dependent quantity is the effective cathode area A. The value of A is governed by the extent of the glow plasma in the interelectrode space, which in turn is determined by a combination of plasma and load conditions. These conditions are discussed in Section II-D.

B. PLASMA TEMPERATURE AND ITS DEPENDENCE ON SPACING AND PRESSURE

The arc drop V_d can be evaluated by equating power input to power losses of the plasma. Under the assumption of zero back emission from the anode, V_d becomes

$$V_d = \frac{2k}{e}\left(T_e - T_c\right)\frac{I_c}{I} + \frac{P_L}{I} \tag{26}$$

where

T_e = electron plasma temperature

I_c = electron current emitted by the cathode into the plasma

P_L = radiation and thermal losses from the plasma.

Due to reverse electron emission from the plasma to the cathode, I_c is larger than the current measured in the external circuit (see Section II-C). The electron temperature T_e can be evaluated from the ball-of-fire theory.[34,35] T_e is determined by

$$\sqrt{\frac{eV_i}{kT_e}}\left(\frac{eV_i}{kT_e}+2\right)^{-1}\exp\left(\frac{eV_i}{kT_e}\right) = \frac{8}{\pi}C_i V_i Q_p\left(\frac{kT_g}{eV_i}\right)^{1/2}\left(\frac{m_p}{m_e}\right)^{1/2}\frac{n_g^2 D^2}{\theta^2} \tag{27}$$

where

V_i = ionization potential

$C_i = \left(\frac{d\,Q_i}{d\,V}\right)_{V = V_i}$

Q_i = ionization cross section

Q_p = ion - atom collision cross section

m_p = ion mass

m_e = electron mass

T_g = average gas temperature in the interelectrode space

n_g = density of gas atoms in the interelectrode space

D = cathode-to-anode spacing

θ = angle in the range $0 < \theta < \pi/2$

Minimum electron temperature occurs for $\theta = \pi/2$. If we assume that the gas density n_g for a cesium vapor converter is related to the vapor pressure p at the cesium reservoir (vapor pressure determined by reservoir temperature) by an arrival rate balance, Eq. (26) becomes

$$\sqrt{\frac{eV_i}{kT_e}}\left(\frac{eV_i}{kT_e}+2\right)^{-1}\exp\left(\frac{eV_i}{kT_e}\right) = \frac{8}{\pi} C_i V_i Q_p \left(\frac{kT_g}{eV_i}\right)^{1/2}\left(\frac{m_p}{m_e}\right)^{1/2}\frac{273^2}{T_g T_R}(3.56\times 10^{16})^2\frac{p^2 D^2}{\theta^2} \tag{28}$$

where

T_R = cesium reservoir temperature.

θ is determined by the relation

$$\frac{\psi_c}{\lambda_e} D \frac{273}{T_g} p_g = \theta \tan\frac{\theta}{2} \tag{29}$$

where

ψ_c = plasma boundary factor $(0 < \psi_c < 1)$

λ_e = electron mean free path at standard gas temperature and pressure (273°K and 1 Torr)

and

p_g = vapor pressure in interelectrode space.

For arrival rate balance Eq. (29) becomes

$$\frac{\psi_c}{\lambda_e} D\sqrt{\frac{273}{T_g}\frac{273}{T_R}}\, p = \theta \tan\frac{\theta}{2} \tag{30}$$

The factor

$$\frac{\psi_c}{\lambda_e}\sqrt{\frac{273}{T_g}\frac{273}{T_R}} = \frac{1}{\Lambda_o} \tag{31}$$

cannot be calculated to a high degree of accuracy but can be obtained from measurements of $(pD)_o$, the value of (pD) corresponding to the minimum electron temperature ($\theta = \pi/2$). Thus

$$(pD)_o = \Lambda \frac{\pi}{2} \tag{32}$$

and Eq. (29) becomes

$$pD = (pD)_o \frac{2}{\pi} \theta \tan \frac{\theta}{2} \tag{33}$$

Using published values for the cesium,[36,37] $Q_p = 6.8 \times 10^{-13}$ cm^2 and $C_i = 6.22 \times 10^{-16}$ cm^2 volt^{-1}, and assuming $T_p = 1130°K$ and $T_R \approx 575°K$, Eq. (28) becomes

$$\sqrt{\frac{45100}{T_e}}\left(\frac{45100}{T_e} + 2\right)^{-1} \exp\left(\frac{45100}{T_e}\right) = 4.95 \times 10^7 \frac{p^2 D^2}{\theta^2} \tag{34}$$

Equations (33) and (34) have been plotted in Fig. 22 with $(pD)_o$ as a parameter. Experimentally, it has been found that $(pD)_o$ = 0.1 to 0.2 Torr x cm. Fig. 22 shows that if the spacing or pressure is increased, the electron temperature decreases and reaches a minimum value corresponding to $(pD)_o$. Further increase in spacing or pressure results in the formation of a second plasma region, separated from the first by a Langmuir space-charge sheath.[34]

C. EFFECTS OF REVERSE CURRENTS

To evaluate the ratio of cathode emission current to terminal current [I_c/I in Eq. (26)] it is necessary to analyze the effects of reverse currents in the converter. It is assumed in this analysis that the concepts of the ball-of-fire discharge apply with the typical potential distribution in Fig. 23.

Two types of back emission currents will be considered namely, I_{pc} from the plasma arriving at the cathode and I_A emitted by the anode into the plasma. The current emitted from the cathode and arriving in the plasma is I_c and the current arriving at the anode from the plasma is I_{pA}. Since the terminal current, I, measured in the external circuit is continuous, the

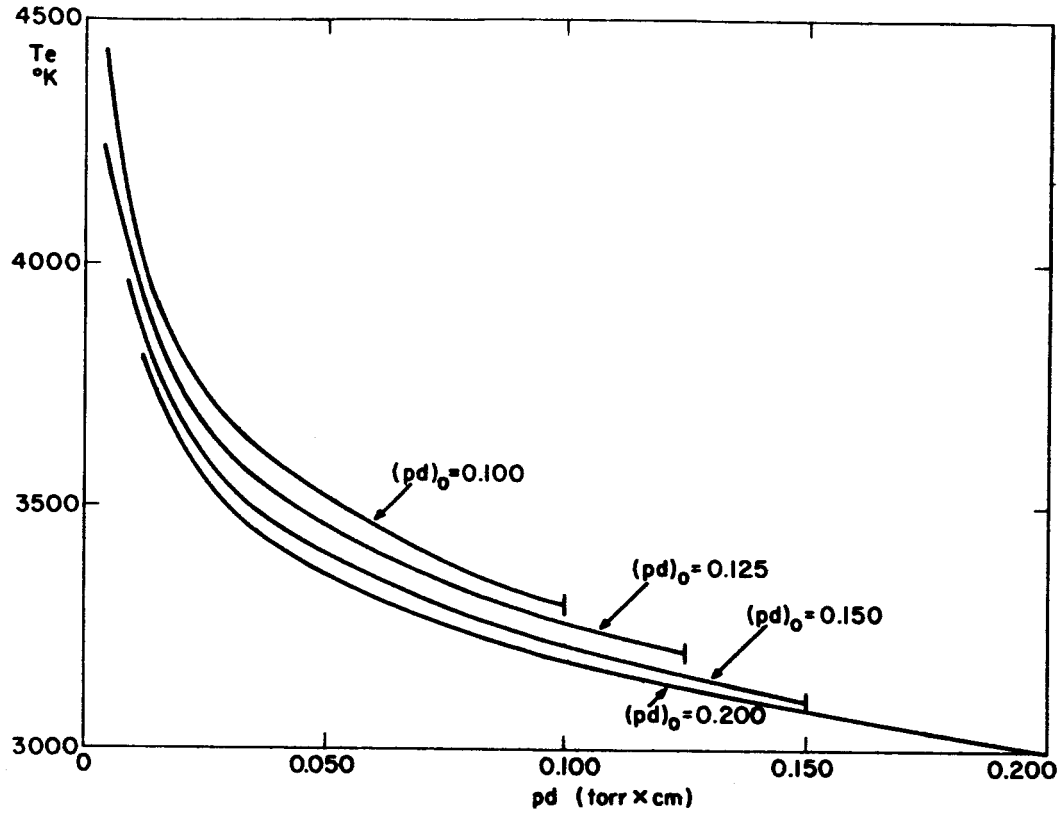

Fig. 22. Electron temperature as a function of the pressure-spacing product.

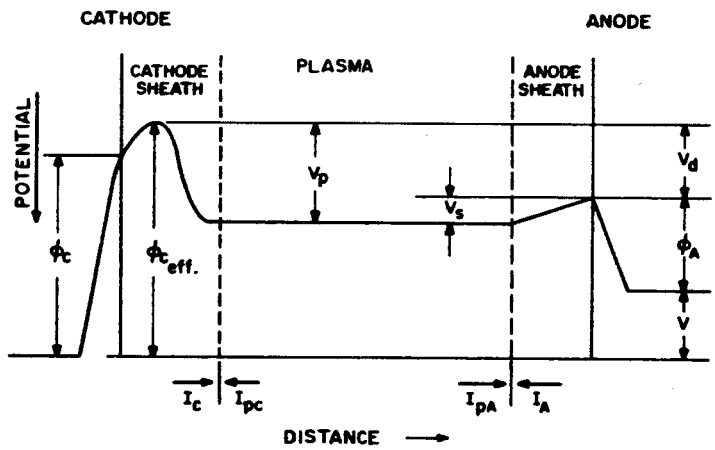

Fig. 23. Diagram showing potential versus distance for an arc mode plasma diode.

following relations apply

$$I = I_c - I_{pc} \tag{35}$$

and

$$I = I_{pA} - I_A \tag{36}$$

where for a plane parallel geometry

$$I_c = ABT_c^2 \exp\left(-\frac{e\,\phi_{ceff}}{kT_c}\right) \tag{37}$$

$$I_{pc} = A\,e\,\Gamma_c \exp\left(-\frac{e\,V_p}{kT_e}\right) \tag{38}$$

$$I_{pA} = A\,e\,\Gamma_A \exp\left(-\frac{e\,V_s}{kT_e}\right) \tag{39}$$

and

$$I_A = ABT_A^2 \exp\left(-\frac{e\,\phi_A}{kT_A}\right) \tag{40}$$

In Eqs. (37) through (40)

B = electron emission constant $\left(=120 \frac{\text{amp}}{\text{cm}^2 \times (^\circ\text{K})^2}\right)$

T_A = anode temperature

ϕ_A = anode work function

Γ_c = plasma electron impact rate (in $\text{cm}^{-2} \times \text{sec}^{-1}$) at cathode edge of the plasma

Γ_A = plasma electron impact rate at anode edge of the plasma.

Equations (35) through (40) can be rearranged to yield

$$I = I_c\left[1 - \left(1 + \frac{\Gamma_A}{\Gamma_c}\exp\frac{e\,V_d}{kT_e}\right)^{-1} - \frac{I_A}{I_c}\left(1 + \frac{\Gamma_A}{\Gamma_c}\exp\frac{e\,V_d}{kT_e}\right)^{-1}\right] \tag{41}$$

showing that the terminal current I is lower than the cathode emission current I_c due to the two reverse emission effects.

In addition to reducing the terminal current the reverse emission also has an undesirable cooling effect on the plasma electrons. This results in an

increased arc drop V_d. The energy balance for the plasma region yields

$$I_c\left(V_p + \frac{2kT_c}{e}\right) - I_{pc}\left(V_p + \frac{2kT_e}{e}\right) - I_{PA}\left(V_s + \frac{2kT_e}{e}\right) + I_A\left(V_s + \frac{2kT_A}{e}\right) - P_L = 0 \tag{42}$$

where P_L represents the small contribution of ion losses, radiation losses, and heat transfer from the electron gas to the neutral gas. Thus from Eq. (42) the arc drop becomes

$$V_d = \frac{2k}{e}\left(T_e - T_c\right)\frac{I_c}{I} + \frac{2k}{e}\left(T_e - T_A\right)\frac{I_A}{I} + \frac{P_L}{I} \tag{43}$$

The quantity $\frac{2k}{e}(T_e - T_c)\frac{I_c}{I}$ of the right-hand side of Eq. (43) represents the heat exchange between plasma and electrodes in absence of anode emission. Since the reverse current from plasma to cathode makes $\frac{I_c}{I} > 1$, it is seen that this effect results in a contribution to the arc drop. The quantity $\frac{2k}{e}(T_e - T_A)\frac{I_A}{I}$ on the right-hand side of Eq. (43) represents the cooling effect on the electron gas due to the anode back emission.

Since the electron impact rates at the two plasma boundaries are proportional to the corresponding plasma densities, one can write for a ball-of-fire type discharge[34]

$$\frac{\Gamma_A}{\Gamma_c} = \cos\theta \tag{44}$$

where θ is determined by Eq. (33). Considering now the case of zero anode emission ($I_A = 0$) and negligible plasma losses P_L, Eqs. (41), (43), and (44) yield

$$\frac{e\,V_d}{kT_e} = 2\left(1 - \frac{T_c}{T_e}\right)\left[1 + \frac{1}{\exp\frac{e\,V_d}{kT_e}\cos\theta}\right] \tag{45}$$

Equations (33), (10), and (45) allow the evaluation of arc drop V_d as a function of pd with $(pd)_o$ as a parameter.

Equations (25) and (41) can be combined to yield

$$V = \frac{kT_c}{e}\ln\frac{120\,A\,T_c^{\,2}}{I} - \frac{kT_c}{e}\ln\left[1 + \frac{\Gamma_c}{\Gamma_A}\exp\left(-\frac{e\,V_d}{kT_e}\right)\right] - \phi_A - V_d \tag{46}$$

If the cathode work function is estimated from Richardson's equation using the current density based on the terminal current, it must be corrected using the second term on the right-hand side of Eq. (46). Often the arc drop is deduced from measurements using the current-independent terms in Eq. (46). This value $(V_d)_{exp}$ is then

$$(V_d)_{exp} = V_d + \Delta\phi_c \tag{47}$$

where

$$\Delta\phi_c = \frac{kT_c}{e} \ln\left[1 + \frac{\Gamma_c}{\Gamma_A} \exp\left(-\frac{e\,V_d}{kT_c}\right)\right] \tag{48}$$

The quantity $(V_d)_{exp} = V_d + \phi_c$ has been plotted in Fig. 24 as a function of pd using Eqs. (33), (34), (45), and (48). Parameter is $(pd)_o$.

The shape of these curves closely resembles that found by Johnson[34] for an xenon discharge having the cathode edge anchored by a grid. Also plotted in Fig. 24 are experimental data for cesium.[38] Allowing $\frac{P_L}{I} \approx 0.050$ volt representing extraneous losses, the curve for $(pd)_o = 0.125$ shows excellent agreement with experiment. The absence of the sharp rise in arc drop before transition into a second glow region for cesium is believed to be due to the fact that in the experiment the cathode edge is not anchored but allows formation of a "dark" plasma in front of the cathode.

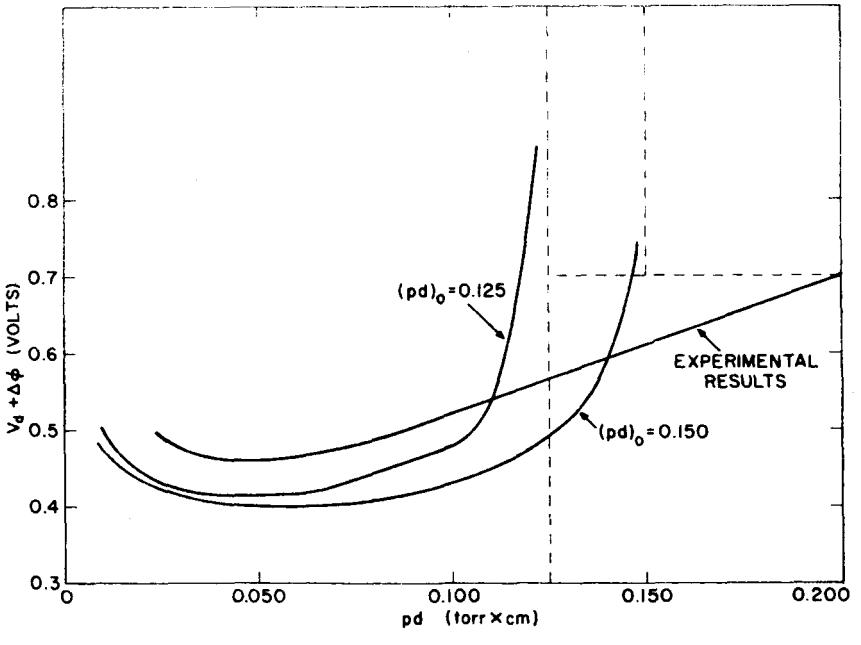

Fig. 24. Arc drop as a function of the pressure-spacing product.

D. RADIATION LOSSES FROM PLASMA

Radiation due to excited atoms in the plasma is generally assumed to be a small contribution to the arc drop.[34] From experiments it is inferred that P_L/I is about 10% of V_d or 50 millivolts of the 1/2 volt arc drop for cesium at high current densities. Power losses due to transitions between higher excited states are proportional to the discharge current. Radiation due to transitions from the resonance states to the ground state (resonance radiation) tend to saturate at higher current densities due to collisions of the second kind.[39] The time rate of change of the density of atoms excited to a certain state can be written as

$$\dot{N}_x = NN_g \int_{\sqrt{\frac{2eV_x}{m_e}}}^{\infty} Q_x \tau_e f(v_e) dv_e - NN_x \int_0^{\infty} Q_q N_e f(v_e) dv_e - \frac{N_x}{\tau} = \tag{49}$$

$$= NN_g \gamma_x - NN_x \gamma_q - \frac{N_x}{\tau}$$

where

N = plasma density

N_g = neutral gas density

Q_x = cross section for excitation by electron impact

v_e = electron velocity

$f(v_e)$ = electron velocity distribution

V_x = excitation potential

m_e = electron mass

N_x = density of excited atoms

Q_q = cross section for quenching of excited atoms by electrons

τ_x = effective average lifetime of excited atoms in plasma region.

γ_x and γ_q represent the two integrals of Eq. (49). Since in general N is proportional to the current density I/A and $\dot{N}_x = 0$ in equilibrium, Eq. (49) yields

$$N_x = \frac{C' I/A \, \gamma_x}{C' I/A \, \gamma_q + 1/\tau} \tag{50}$$

where C' is a constant. The power lost from the plasma (neglecting side losses) becomes

$$P_L = eV_x \frac{N_x}{\tau_x} A D \tag{51}$$

Thus summing up contributions of different excited

$$\frac{P_L}{I} = \sum_x e V_x D \frac{C' \gamma_x}{\tau_x C' \gamma_q I/A + 1} \tag{52}$$

Considering the resonance states separately (τ_x large due to resonance absorbtion), Eq. (52) can be written

$$\frac{P_L}{I} = \frac{1}{C'' + C''' I/A} + \frac{P_L'}{I} \tag{53}$$

where C'' and C''' are constants and P_L' corresponds to radiation losses other than resonance radiation. Consequently, the volt-ampere characterestic [Eqs. (25) and (48)] becomes

$$V \cong \frac{kT_c}{e} \ln \frac{120\ T_c^2}{I/A} - \frac{1}{C'' + C''' I/A} - V_d - \phi_A \tag{54}$$

At high current densities the term corresponding to the resonance radiation becomes vanishingly small. At lower current densities this term causes a deviation from linearity in a log I versus V plot. At current densities much lower than the saturated cathode emission current density the effective emission area A can vary because the size of the glow plasma varies. A is determined by setting the derivative of Eq. (54) equal to zero, or

$$\left.\frac{\partial V}{\partial I}\right|_{\frac{V}{I} = \text{const} = R} = 0 \tag{55}$$

where R = load impedance.

E. EFFECTS OF NOBLE GAS ADDITIVES ON THE PERFORMANCE OF THERMIONIC CONVERTERS

Noble gases added to a cesium vapor thermionic converter have two effects on the plasma properties of the device. One is a change of the transport pro-

perties for the electrons through the diode. This effect can be incorporated as a correction term in Eq. (27) relating the electron temperature and diode spacing. The other effect is the energy loss for the electron gas due to electron-gas atom collisions. This effect will be evaluated by considering the energy loss per collision and summing up all electron-gas collisions per unit time.

For conditions of interest for thermionic converters, the electron temperature is so low that ionization of the added (noble) gas can be neglected. Thus, only elastic collisions of electrons and ions with the added gas need be considered. It is convenient to write for the total electron-atom collision probability (including both electron collisions with cesium and with the added gas)

$$(Q\ N_g)_{tot} = Q_e\ n_g + Q_{ea}\ n_a = Q_e\ n_g\ (1 + \frac{n_a}{n_g}) \tag{56}$$

where

Q_e = electron-cesium atom collision cross section
$= \lambda_e \times (3.56 \times 10^{16})^{-1}$
Q_{ea} = electron-atom collision cross section for the added gas
n_a = density of added gas
$\alpha = n_a/n_g$

Similarly for ion-atom collisions

$$(Q\ N_g)_{tot_p} = Q_p\ n_g\ (1 + \alpha \frac{Q_{pa}}{Q_p}) \tag{57}$$

where

Q_{pa} = cross section for collisions between cesium ions and atoms of added gas.

Equations (32) and (34) may thus be written

$$(pD)_o = \frac{\pi}{2} \frac{\lambda e}{\psi_c} \sqrt{\frac{T_g\ T_R}{273}} \quad \frac{1}{1 + \alpha \frac{Q_{ea}}{Q_e}} \tag{58}$$

and

$$\sqrt{\frac{45100}{T_e}} \left(\frac{45100}{T_e} + 2\right)^{-1} \exp\left(\frac{45100}{T_e}\right) = 4.95 \times 10^7 \frac{p^2 D^2}{\theta^2} \left(1 + \alpha \frac{Q_{pc}}{Q_p}\right) \tag{59}$$

Using Eqs. (58), (58), (33), and (45) the relationship between arc drop V_d and pD may now be evaluated for different concentrations of gas additives (α). It is planned to make numerical evaluations of these equations. Since θ is changed by adding gases, both the arc drop and the available terminal current [Eq. (41)] will be affected.

In elastic collisions between electrons and atoms the average energy transfer from the electron to the atom is $= 2\frac{m_e}{m_p}$ times the electron energy. Thus the power transfer from the electron gas to the added gas becomes

$$P_R = \int_0^D dx \int_0^\infty N\, n_a\, Q_{ea} \frac{m_e^2}{m_p}\, v_e^3\, f(v_e)\, dv_e \qquad (60)$$

per unit cathode area. If Q_{ea} is velocity-independent, Eq. (59) becomes

$$P_R = \frac{16}{\sqrt{2\pi}}\, n_a\, Q_{ea}\, \frac{m_e^2}{m_p} \left(\frac{kT_e}{m_e}\right)^{3/2} \int_0^\Delta N\, d\, x. \qquad (61)$$

III. EXPERIMENTAL PLASMA STUDIES

A. INTRODUCTION

Two experimental approaches to plasma voltage drop may be distinguished. The first involves measurement of electron temperature and calculation of plasma voltage drop (arc drop) from energy balance considerations. The second approach is more direct and requires that the arc drop be related to measured terminal voltage. This may be done provided that virtual cathode and anode work function potential barrier heights are known. With certain tenable assumptions, the virtual cathode barrier height may be readily calculated from the observed terminal current. The remaining problem of obtaining a known anode work function is discussed in some detail.

B. PROBE MEASUREMENT OF ELECTRON TEMPERATURE IN A CESIUM PLASMA

Langmuir probe techniques are well known[40] and have been employed successfully for measurement of electron and ion temperature and density in various types of plasma. Two severe problems have limited the application of probe techniques to cesium plasma: (1) There is the difficulty of cooling a probe enough to make thermionic emission negligible. (2) There is the leakage current due to cesium adsorption on the necessary probe support and feedthrough insulators.

The probe structure shown in Fig. 25 was designed in an attempt to minimize these difficulties. Thermal contact between probe and anode maintains the probe

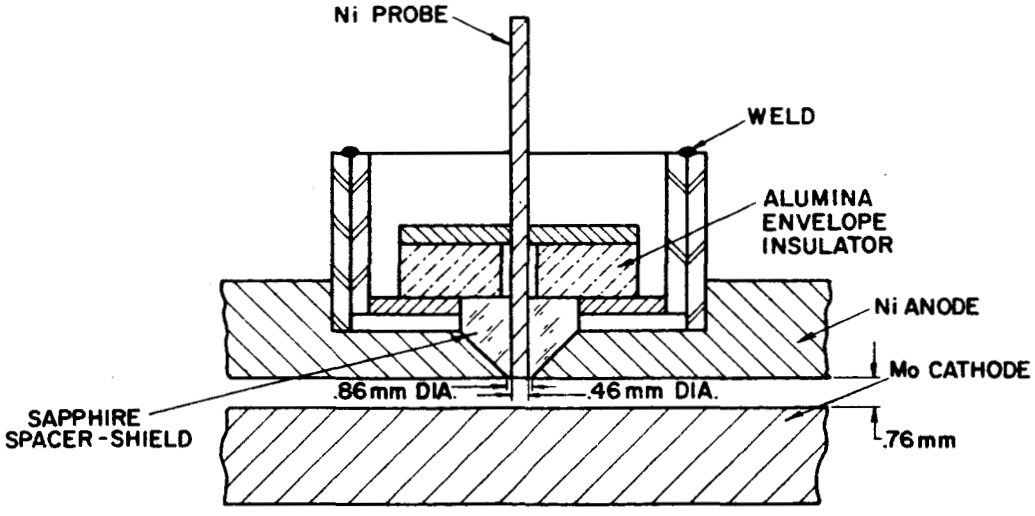

Fig. 25. Details of probe assembly.

at the relatively low anode temperature, for low thermionic emission. The emission which comes from the probe side is impeded by the conically shaped sapphire spacer-shield. The anode-probe area ratio was 1580. Cathode area was 2.5 cm^2.

In operation, the anode-probe temperature was set at a value which represented a compromise between probe thermionic emission and probe insulator leakage.

Two separate but synchronized pulsers were used to obtain probe characteristics. Rectangular pulses of about 5-msec duration were applied to the anode at a repetition rate of 7.5, 15 or 30 pps. The probe characteristic was plotted 60 times each second using a half-wave rectifier connected to the power line through a small transformer. Raw data are shown in Fig. 26. The low-current, constant-slope base-line gives a convenient indication of leakage current, which

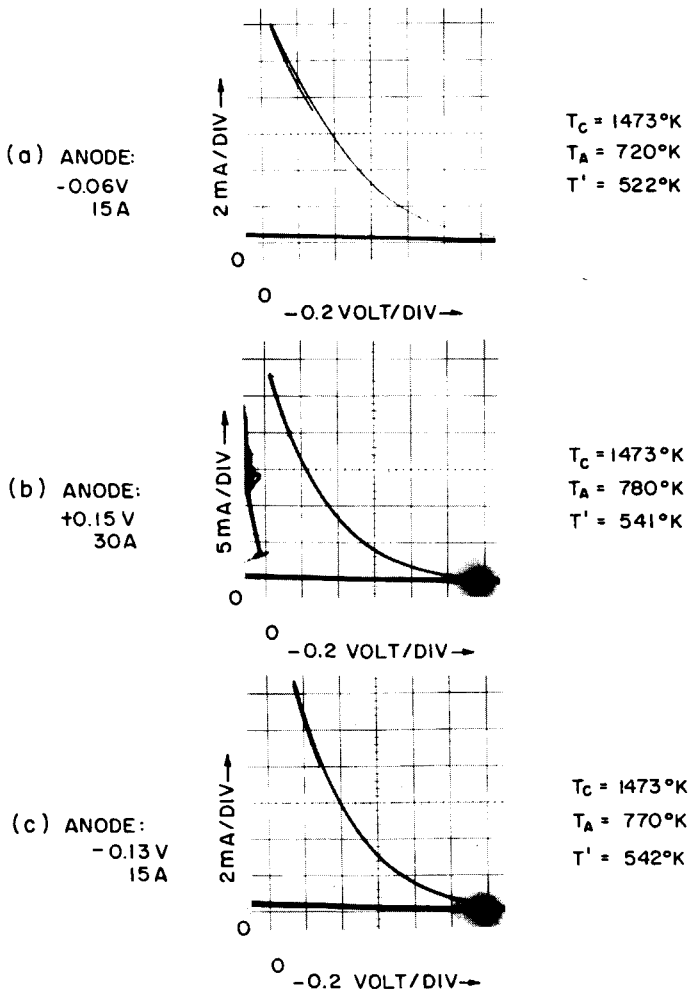

Fig. 26. Oscillograms showing probe characteristics. Voltages are measured with respect to the cathode terminal.

flows during power line cycles in which the arc remains extinguished. Probe data are replotted in Fig. 27. From the slopes, electron temperatures in the range 3000-4000°K are indicated.

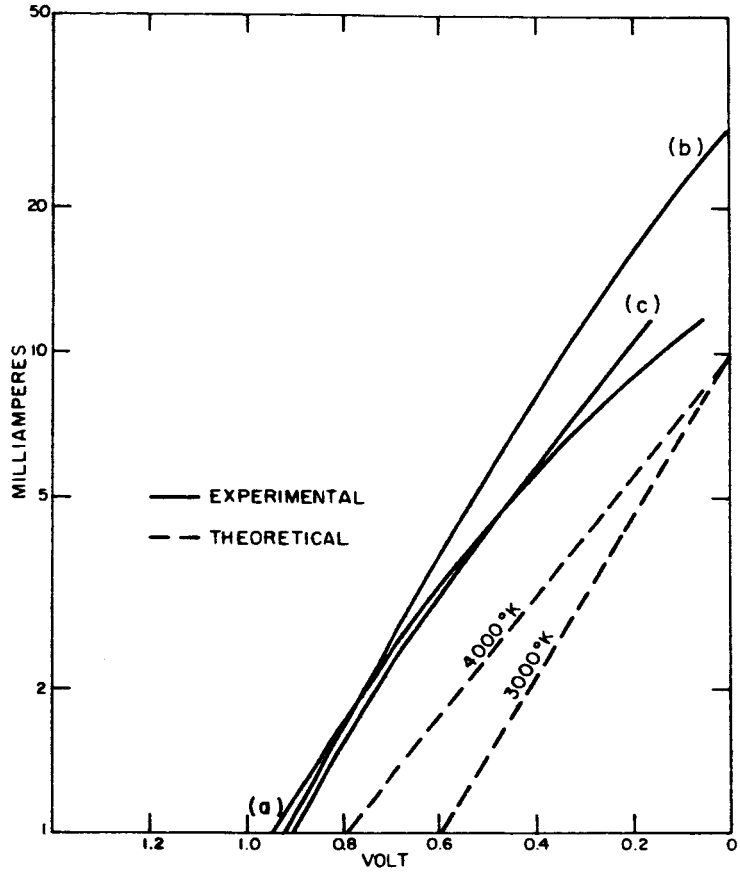

Fig. 27. Re-plot of data of Fig. 26.

Compared with desired electron current values, the probe leakage current value was small. However, attempts at interpreting negative probe characteristics were futile. It was found that ion current was masked by probe thermionic emission, whenever the probe temperature was raised high enough for negligible insulator surface leakage.

Before systematic measurements of electron temperature variation with pressure, spacing, and current could be accomplished, the probe assembly developed a vacuum leak, and the tube had to be disassembled.

Nevertheless, it is interesting to note the consistency of the electron temperature measurements reported here with electron temperatures calculated from cross-sectional data or deduced from arc drop measurements.

C. DISCUSSION OF METHODS FOR ARC DROP MEASUREMENTS

Arc drop in a cesium diode may be measured if the anode work function is known. It is given approximately by

$$(V_d)_{exper.} = \frac{kT_c}{e} \ln \frac{ABT_c^2}{I} + V - \phi_A , \qquad (62)$$

where V is the anode-to-cathode terminal voltage.

The other symbols were defined in Section II. There it was shown that the arc drop so measured is not precisely the "true arc drop" defined by the potential distribution diagram in Fig. 23. However, for simplicity, and in order to permit ready comparison with arc drop data of other workers, there are listed in this section only experimental values of V_d calculated from Eq. (62). If desired, a small correction ($\triangle\phi_c$) may be subtracted to obtain the true arc drop.

One method for estimating anode work function has been described by Kitrilakis, Shavit, and Rasor.[38] They measured anode work function with the tube operating as an ion-rich surface ionization diode and plotted ϕ_A vs. T_A/T'. Then they assumed that the same relation held for the higher cesium reservoir temperature T' required for arc mode operation.

Another method is to lower the anode temperature as close as possible to T', and then assume that anode work function is equal to that of bulk cesium, which is here taken to be 1.96 volts. Evidence for this value is given in Section III-G.

The latter method is preferred. Experiments indicate variation in the minimum anode work function of the order of 0.1 volt, depending upon the thermal and cesium coverage history. The anode work function at maximum coverage attainable in our experimental tube was found to be reproducible within 10 or 20 millivolts, and seemed to be less dependent upon previous processing. Another reason for preferring the high-coverage, low-anode temperature condition for arc drop measurements is that under such conditions thermionic emission from the anode is negligible. Theory detailed in Section II-C shows that converter optimization may involve acceptance of an additional arc drop term due to reverse current from the anode surface.

D. EXPERIMENTAL TUBE DESCRIPTION

All arc drop and anode work function experiments reported in this section employed a planar diode with a 2.5 cm^2 cathode area. A stainless steel bellows was included for adjustment of the anode-to-cathode spacing.

A ceramic shield (Morganite RR alumina) was installed around the cathode side walls to impede transmission of the copious electron current that is emitted from the sides of the Mo cathode button, and from the side of the Mo heat dam. The gap between shield and cathode was about 0.1 mm. A "blackbody" hole in the cathode button was lined up with a corresponding hole in the ceramic shield, and cathode temperature was measured with an optical pyrometer, sighting through a sapphire window. All temperature readings were corrected for reflection losses at the window.

The anode was machined from nickel rod (INCO 270).

E. RESIDUAL GAS PUMPING AND ANALYSIS

The experimental tube was continuously pumped using a cesium still, cold trap and getter-ion pump arrangement which has been previously described.[41] Partial pressures of residual gases were monitored from time to time with a mass spectrometer having partial pressure sensitivity of about 10^{-10} Torr. A Bayard-Alpert ionization gauge was also included in the system. Ultimate pressure attained was about 3×10^{-10} Torr total pressure in the high vacuum section, with the cesium still and experimental tube at room temperature. Typical pressure at the B-A gauge during arc mode operation was 5×10^{-8} Torr, which was mostly hydrogen.

F. EXPERIMENTAL PROCEDURES IN ARC DROP MEASUREMENTS AND DISCUSSION OF POSSIBLE ERRORS

Unfortunately, the experimental tube design was such that multilayer cesium coverage on the anode surface could not be easily attained. The problem was that the anode side wall surface cooled faster, and to lower temperatures than the electron collection surface. A spurious cesium reservoir would form on the anode side whenever the anode temperature T_A was within about 15°C of the proper reservoir temperature T'. Additional lowering of T_A would result in a lower effective reservoir temperature.

The procedure finally adopted was to slowly cool the anode, and take arc drop data at the first indication of bulk cesium transport to the spurious reservoir. Several useful indications of bulk cesium transport were observed.

First, a decrease in partial pressure of hydrogen gas would be observed at the mass spectrometer. The flow of cesium from the still boiler (proper reservoir) to the experimental tube (spurious reservoir) resulted in diffusion pumping of residual hydrogen gas toward the tube. Since hydrogen was the predominant residual gas observed in the high vacuum section of the system, an ordinary ion gauge could be used as well as the mass spectrometer for an indicator of spurious reservoir formation.

A few seconds after the diffusion pumping indication, one could observe a drop in temperature of the proper reservoir, due to evaporation cooling.

A third indication of spurious reservoir formation is had when one is operating under emission-limited conditions. Under such conditions, a lowering of cesium pressure results in a large increase of anode terminal voltage needed to maintain constant current through the diode.

The experimental tube had no potential probe on the cathode proper. Cathode heat dam resistance was estimated at 1.5 milliohm, and the indicated terminal voltage was corrected appropriately. Using published data on the absolute thermoelectric power of molybdenum,[42] a heat dam thermal emf correction of 20 millivolts was applied. The Joule and Seebeck voltages introduced errors which were partly compensated, and both might be neglected without much error.

Probably the largest error in these experiments, and one which is difficult to estimate accurately, involves the knowledge of effective area. The geometric area of the cathode end face was very nearly 2.5 cm^2. It was visually apparent, however, that the glow in the planar region was concentrated toward the center. Uniformity was better at higher current density, and the high current density measurements should therefore be given more weight. Also, the uniformity was better at closer spacings.

A possible explanation for nonuniformity is this: Near the outer radius of the cathode, cesium arrival rate and gas density are given approximately by pressure balance considerations, whenever the bath temperature is high enough for cesium-cesium collisions to be important. The center region has relatively poor conductance to the reservoir, and here arrival rate balance with the reservoir may always be assumed. These considerations show that arrival rate and gas density are always highest at the center.

G. ARC DROP MEASUREMENT RESULTS

Experimental values of arc drop are plotted in Fig. 28. The points represent data taken with cesium bath temperatures in the range 501-577°K and actual spacing from 0.25 to 1.25 mm. The data show slightly higher arc drop at the lower cathode temperatures, in qualitative agreement with theory. Anode temperature in all cases was not over 25°C higher than the cesium reservoir temperature, and the anode work function was taken to be 1.96 volts.

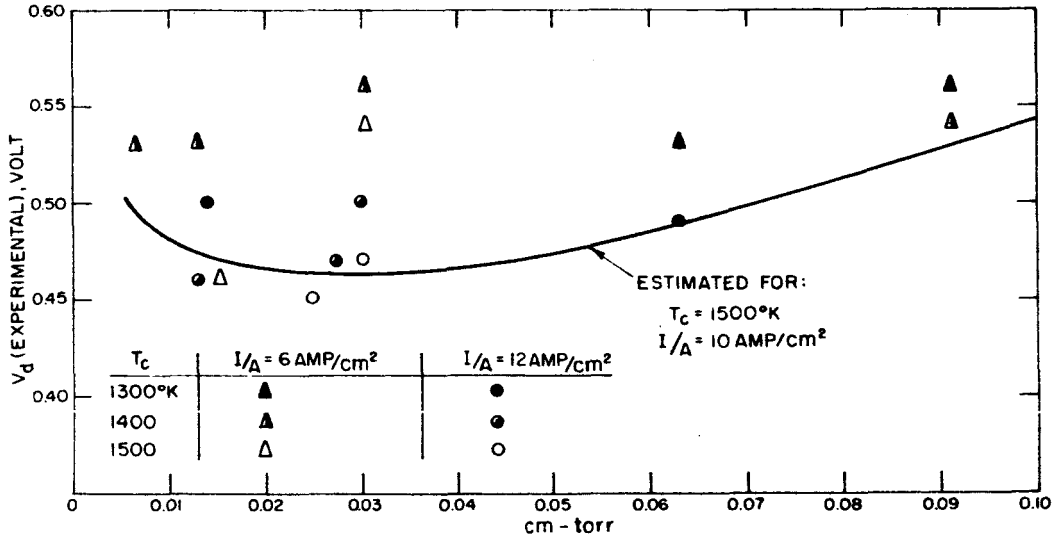

Fig. 28. Experimental arc drop as a function of spacing-pressure product.

H. WHAT IS THE WORK FUNCTION OF CESIUM?

The literature (to our knowledge) is not in good agreement concerning the work function of cesium. Kingdon[43] published some thermionic emission data in an abstract. His data are presumably the basis for the widely quoted value of 1.81 volts, although substitution of his data in Richardson's equation yields somewhat lower effective work function values. Kingdon mentioned an impurity effect and was himself reluctant to extract work function values from his reported data.

Data on photoemission from cesium films is reported by Brady.[44] The fit with Fowler's theoretical curve[45] is not very satisfactory, but a value of 1.97 volts is indicated by his "10 molecular layer" data. Mayer[46] also did photoemission experiments, and he reports a value of 1.94 volts as the work function for a thick film of cesium.

In an attempt to resolve doubts about the work function of cesium, we made measurements of anode work function by operating the experimental tube in an ion-rich, low-pressure surface ionization mode. Dynamic equilibrium cesium coverage of the anode was made as large as possible, to closely approach an anode work function equal to that of bulk cesium. Terminal voltage was measured to within 10 millivolts, and a correction of 20 millivolts was applied to account for the Seebeck voltage (thermal emf) developed in the cathode heat dam made from molybdenum. This material has a slightly positive absolute thermoelectric power.[42] The heat dam temperature distribution therefore enhanced electron current flow in the diode, and required that an absolutely greater retarding potential be applied for a given diode current. Anode work function was calculated from

$$\phi_A = \frac{kT_c}{e} \ln \frac{ABT_c^2}{I} - |V| + 0.02 \text{ volt} \qquad (63)$$

where V is the observed terminal voltage.

Typical results for ϕ_A vs. I/A are plotted in Fig. 29. Note that the apparent ϕ_A increases for large values of I. This is the result of certain areas becoming electron- or ion-emission limited. Under such conditions, the

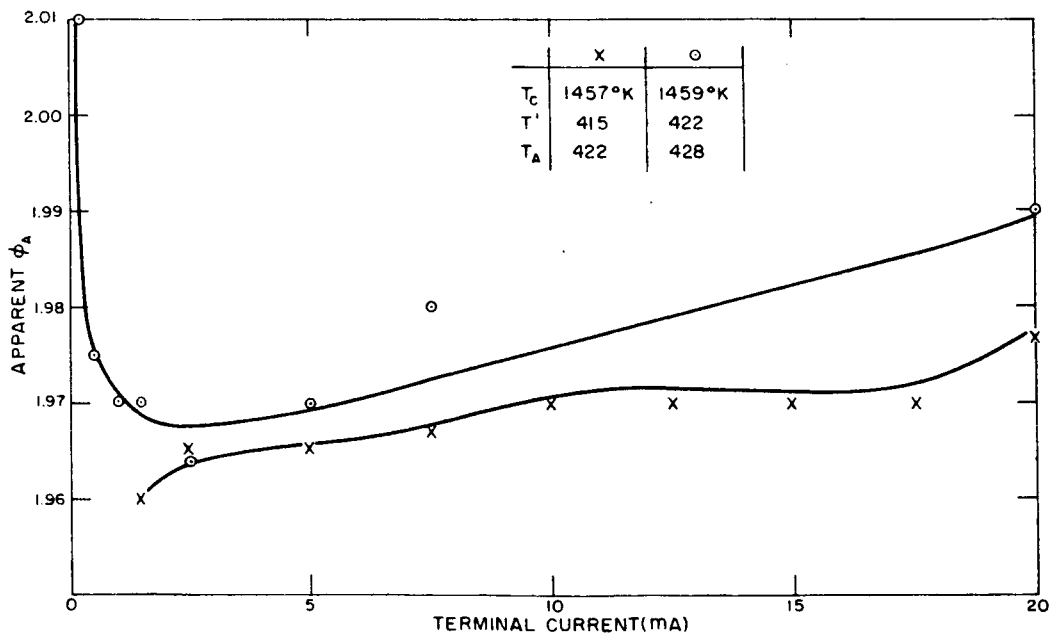

Fig. 29. Apparent anode work function in a surface ionization diode as a function of terminal current.

error lies in taking the geometric area A as the effective area. When ϕ_A is calculated with very low I/A, the apparent ϕ_A again increases. Here the error lies in assuming that electron current is equal to terminal current. At low terminal currents, the unknown ion current becomes significant. One is justified, therefore, in concluding that ϕ_A is at least as low as indicated by Eq. (62). A detailed analysis of cathode work function distribution, deduced from saturated electron and ion current, proves that operation with a virtual cathode (retarding potential) allows one to set an upper limit on emission-limited area. When this is done, it is seen that for values of I/A near minimum apparent ϕ_A, the doubtful area is about 10% of the total area. The result of several high coverage determinations of minimum apparent ϕ_A was 1.96 ± 0.01 volt. Emission-limited area uncertainties lead one to write $1.96 \begin{smallmatrix} + 0.01 \\ - 0.02 \end{smallmatrix}$ volt. Possible cathode temperature measurements errors of $\pm$ 5°K give a final result of $1.96 \begin{smallmatrix} + 0.02 \\ - 0.03 \end{smallmatrix}$ volt.

Collision losses were neglected, since it was found that halving or doubling the cesium pressure changed results by less than 5 millivolts.

The most serious uncertainty in these measurements is the precise difference between anode temperature T_A and cesium reservoir temperature T'. Thermal radiation from the cathode is the principal heat input, and this falls on the end face of the anode, which is the electron-bombarded surface, or anode proper. The cooling air, however, hits the side wall of the nickel anode, as well as the end face. Because the heat input to the side wall is slight, the side surface cools below the end face temperature. The result is that bulk condensation always begins at the side. Because of thermal resistance in the nickel cup, a temperature difference of about 15°C was usually present. Therefore, the detailed behavior of anode work function in the high coverage region could not be investigated. It is thought that the highest coverages attained gave anode work function equal to that of bulk cesium, but there is no certainty on this point. Assuming only that there exists no maximum in the anode work function vs. temperature curve, one can conclude from measurements reported here that

$$\phi_{Cs} \geq 1.93 \text{ volts} \tag{64}$$

On the basis of known data a value of $\phi_{Cs} = 1.96$ volts is recommended.

Present day ultra-high vacuum techniques should be used for a new photoelectric measurement of ϕ_{Cs}. An interesting possibility is the use of a red (6328Å) He-Ne gas laser as a light source. Photons from such a laser have energy of 1.96 ev. Hughes and DuBridge[47] have described a method, based on Fowler's theory, in which the light photon energy is kept constant while photoemitter temperature is varied. One thereby avoids the need for adjusting light source intensity as wavelength is varied. A laser source should make it easy to confine illumination to a bulk cesium region and avoid emission from low work function partial coverage regions.

IV. SUMMARY AND CONCLUSION

Electrical conduction associated with adsorption of cesium on insulators has been measured under a wide range of conditions. Empirical formulas were found which represent the data. These formulas should permit a design of cesium vapor devices with acceptably low insulator surface leakage. Understanding of cesium adsorption on insulators is expected to lead to a better understanding of cesium adsorption on other types of substrate.

Theory and experiment on plasma voltage drop in the arc mode thermionic converter are in very good agreement. An arc drop of nearly 0.5 volt seems to be unavoidable. This arc drop is rather insensitive to pressure, spacing, cathode temperature, and current density variation.

The theory now allows prediction of performance of arc mode converters as a function of surface properties. Or, if converter performance has been measured, the theory allows one to deduce surface work function values.

REFERENCES

1. P. B. Weisz, "Electronic Barrier Layer Phenomena in Chemisorption and Catalysis," J. Chem. Phys. 20, 1483 (1952); and "Effects of Electronic Charge Transfer Between Adsorbate and Solid on Chemisorption and Catalysis," J. Chem. Phys. 21, 1531 (1953).

2. V. B. Sandomirskii and Sh. M. Kogan, "Calculation of Adsorption Isotherms in the Electronic Theory of Chemisorption," Russian J. Phys. Chem. 33, 122 (1959).

3. Sh. M. Kogan, "Statistics of Adsorbed Particles in the Electronic Theory of Chemisorption," Zhur. Fiz. Khim. 33, 156 (1959).

4. H. J. Krusemeyer and D. G. Thomas, "Adsorption and Charge Transfer on Semiconductor Surfaces," J. Phys. Chem. Solids 4, 78 (1958).

5. G. Heiland, "Surface Conductivity of Semiconductors and its Variation by Adsorption, Transverse Electric Field, and Irradiation," Disc. Far Soc. 28, 168 (1959).

6. M. Boudart, "Electronic Chemical Potential in Chemisorption and Catalysis," J. Am. Chem. Soc. 74, 1531 (1952).

7. N. F. Mott and R. W. Gurney, Electronic Processes in Ionic Crystals, (Clarendon Press, Oxford, 1940).

8. D. A. Dowden, "Heterogeneous Catalysis. Part I. Theoretical Basis," J. Chem. Soc. (London), 242 (1950).

9. F. F. Vol'kenshtein, The Electronic Theory of Catalysis on Semiconductors, (Macmillan Co., New York, 1963).

10. P. Benjamin and C. Weaver, "Condensation Energies for Metals on Glass and other Substrates," Proc. Roy. Soc. 252A, 418 (1959).

11. T. N. Rhodin, "Oriented Arrangements of Thin Aluminum Films Formed on Ionic Substrates," Disc. Faraday Soc. 5, 215 (1949).

12. J. Frenkel, "Theorie der Adsorption and verwandter Erscheinungen," Z. Phys. 26, 117 (1924).

13. D. Walton, "Nucleation of Silver on Sodium Chloride," J. Chem. Phys. 33, 2698 (1963).

14. C. A. Neugebauer and M. B. Webb, "Electrical Conduction in Ultra-thin, Evaporated Metal Films," J. Appl. Phys. 33, 74 (1962).

15. N. G. Nifontoff, "Some Electrical Properties of Very Thin Metal Films," Bull Acad. Sci. USSR 25, 665 (1961).

16. A. C. B. Lovell, "The Electrical Conductivity of Thin Metallic Films I - Rubidium on Pyrex Glass Surfaces," Proc. Roy. Soc. A157, 311 (1936); and E. T. S. Appleyard and A. C. B. Lovell, "Part II - Cesium and Potassium on Pyrex Glass Surfaces," Proc. Roy. Soc. A158, 718 (1937).

17. E. M. Conwell, "Impurity Band Conduction in Germanium and Silicon," Phys. Rev. 103, 51 (1956).

18. B. L. Blackford, Electronic Research Laboratory, MIT, Quarterly Progress Report 68, 2 (1963).

REFERENCES (Continued)

19. J. D. Levine, "Cesium Adsorption on Insulators," pp. 17-25, Final RCA Report under Contract NAS 3-2531 (Dec. 1963). NASA CR-54009.

20. "The Development of an Auxiliary Electrode Thermionic Converter," Technical Documentary Report No. ASD-TDR-63-442, May 1963. Prepared under Contract No. AF33(657)-8005, pp. 144-145.

21. W. Baltensperger, "On Conduction in Impurity Bands," Phil. Mag. 44, 1355 (1953).

22. C. Erginsov, "Energy States of Overlapping Impurity Centers in Semiconductors," Phys. Rev. 88, 893 (1952).

23. L. W. Swanson, R. W. Strayer, E. C. Cooper, and F. M. Charbonier, "Research on the Behavior of Thin Alkali-Metal Layers on Refractory Metal Substrates," Field Emission Corporation Annual Report (1963), on Contract NASw-458, p. 8.

24. W. Shockley, Electrons and Holes in Semiconductors (Van Nostrand Co., Princeton, 1963) p. 228.

25. G. L. Pearson and J. Bardean, "Electrical Properties of Pure Silicon and Silicon Alloys Containing Boron and Phosphorus," Phys. Rev. 75, 865 (1949).

26. C. Feldman, "Temperature Dependency of Resistance of Thin Films," J. Appl. Phys. 34, 1710 (1963).

27. L. Y. Wei, "Electrical Conductivity of Potassium Films on Potassium Chloride," J. Chem. Phys. 39, 2709 (1963).

28. J. Crank, The Mathematics of Diffusion (Clarendon Press, Oxford, 1956) p. 30.

29. S. Dushman and J. M. Lafferty, Scientific Foundations of Vacuum Technique (Wiley and Sons, Inc., New York, 1962) p. 583.

30. A. J. Learn and R. S. Spriggs, "Behavior of Film Conductance During Vacuum Deposition," J. Appl. Phys. 34, 3012 (1963).

31. F. J. Morin, "Electrical Properties of NiO," Phys. Rev. 93, 1199 (1954).

32. W. Ehrenberg, Electric Conductance in Semiconductors and Metals (Clarendon Press, Oxford, 1958) pp. 72-77.

33. K. G. Hernqvist, Proc. IEEE 51, 748 (1963).

34. E. O. Johnson, RCA Rev. 16, 498 (1955).

35. J. R. Fendley and K. G. Hernqvist, Proc. IEEE 52, 964 (1964).

36. R. H. Bullis, "Report on Thermionic Conversion Specialist Conference at Gatlinburg, Tenn." p. 1, 1962.

37. W. B. Nottingham, Advanced Energy Conversion 3, 245 (1963).

38. S. S. Kitrilakis, A. Shavit, and N. S. Rasor, "Report on 24th Annual Conference on Physical Electronics," MIT, Cambridge, Mass., p. 171, 1964.

39. C. Kenty, J. Appl. Phys. 21, 1309 (1950).

REFERENCES (Continued)

40. See, for example, J. D. Cobine, Gaseous Conductors (Dover Publishing Co., New York, 1958) p. 134.

41. J. R. Fendley, Jr., Rev. Sci. Instr. 35, 905 (1964).

42. Landolt-Börnstein Zahlenwerte und Funktionen..., 6th edition, Vol. II, Part 6, (Springer Verlag, Berlin, 1959) p. 935.

43. K. H. Kingdon, Phys. Rev. 35, 892 (1925).

44. J. J. Brady, Phys. Rev. 41, 613 (1932).

45. R. H. Fowler, Phys. Rev. 38, 45 (1931).

46. H. Mayer, Ann. Physik 33, 419 (1938).

47. A. L. Hughes and L. A. DuBridge, Photoelectric Phenomena (McGraw Hill Book Company, Inc., New York, 1932) p. 248.